(4)

NWC TP 6941

# Scattering Representation of Waveguide/Cavity Discontinuities Using Mode-Matching and the Least Squares Boundary Residual



by
P. L. Overfelt
*Research Department*

OCTOBER 1988

NAVAL WEAPONS CENTER
CHINA LAKE, CA 93555-6001

# Naval Weapons Center

## FOREWORD

The research described in this report was performed at the Naval Weapons Center during fiscal years 1986 through 1988 and was supported by 6.2 Independent Exploratory Development and 6.1 Independent Research funds.

This report is intended to be a working document showing full detail of scattering from waveguide discontinuities. It is primarily intended for those in the radio frequency, microwave, and electromagnetics communities who have need of a detailed analysis method that can be applied to many different and specific type of scattering problems. Computer codes for the two examples in this report are available from the author.

The report has been reviewed for technical accuracy by D. J. White.

Approved by
R. L. DERR, *Head*
*Research Department*
28 April 1988

Under authority of
J. A. BURT
Capt., U.S. Navy
*Commander*

Released for publication by
G. R. SCHIEFER
*Technical Director*

NWC Technical Publication 6941

Published by . . . . . Technical Information Department
Collation . . . . . Cover, 27 leaves
First printing . . . . . 60 copies

# REPORT DOCUMENTATION PAGE

| | |
|---|---|
| 1a. REPORT SECURITY CLASSIFICATION<br>UNCLASSIFIED | 1b. RESTRICTIVE MARKINGS |
| 2a. SECURITY CLASSIFICATION AUTHORITY | 3. DISTRIBUTION/AVAILABILITY OF REPORT<br>A Statement; public release; distribution unlimited. |
| 2b. DECLASSIFICATION/DOWNGRADING SCHEDULE | |
| 4. PERFORMING ORGANIZATION REPORT NUMBER(S)<br>NWC TP 6941 | 5. MONITORING ORGANIZATION REPORT NUMBER(S) |
| 6a. NAME OF PERFORMING ORGANIZATION<br>Naval Weapons Center<br>6b. OFFICE SYMBOL (*If applicable*) | 7a. NAME OF MONITORING ORGANIZATION |
| 6c. ADDRESS (*City, State, and ZIP Code*)<br>China Lake, CA 93555-6001 | 7b. ADDRESS (*City, State, and ZIP Code*) |
| 8a. NAME OF FUNDING SPONSORING ORGANIZATION<br>Naval Weapons Center<br>8b. OFFICE SYMBOL (*If applicable*) | 9. PROCUREMENT INSTRUMENT IDENTIFICATION NUMBER |
| 8c. ADDRESS (*City, State, and ZIP Code*)<br>China Lake, CA 93555-6001 | 10. SOURCE OF FUNDING NUMBERS<br>PROGRAM ELEMENT NO: 62936N; PROJECT NO:; TASK NO: RV36I20; WORK UNIT ACCESSION NO: 906019 |

11. TITLE (*Include Security Classification*)
SCATTERING REPRESENTATION OF WAVEGUIDE/CAVITY DISCONTINUITIES USING MODE-MATCHING AND THE LEAST-SQUARES BOUNDARY RESIDUAL (U)

12. PERSONAL AUTHOR(S)
Overfelt, P. L.

| 13a. TYPE OF REPORT | 13b. TIME COVERED | 14. DATE OF REPORT (*Year, Month, Day*) | 15. PAGE COUNT |
|---|---|---|---|
| Final | FROM 1986 TO 1988 | 1988, October | 52 |

16. SUPPLEMENTARY NOTATION

| 17. COSATI CODES | | | 18. SUBJECT TERMS (*Continue on reverse if necessary and identify by block number*) |
|---|---|---|---|
| FIELD | GROUP | SUB-GROUP | Waveguide Discontinuities, Scattering, Mode-Matching, Least-Squares, Boundary Residual, Evanescent Modes, Modal Reflection, Transmission Coefficients |
| 12 | 01 | | |
| | | | |

19. ABSTRACT (*Continue on reverse if necessary and identify by block number*)

(U) In this report, a scattering matrix representation of waveguide discontinuities using mode-matching and the least-squares boundary residual is developed. The method is applied to two simple problems: (1) The thin capacitive iris junction in a parallel-plate waveguide and (2) the asymmetric H-plane parallel-plate waveguide step. Results for satisfaction of both tangential and normal boundary conditions, the error function associated with a particular set of modes, the dominant mode reflection and transmission coefficients, and the numbers of modes used as well as the modal ratios, are presented. It is shown that the method avoids relative convergence, includes evanescent modes explicitly, exhibits slow but guaranteed convergence, and exhibits numerical stability and excellent accuracy.

| 20. DISTRIBUTION/AVAILABILITY OF ABSTRACT | 21. ABSTRACT SECURITY CLASSIFICATION |
|---|---|
| ☐ UNCLASSIFIED/UNLIMITED ☒ SAME AS RPT ☒ DTIC USERS | Unclassified |
| 22a. NAME OF RESPONSIBLE INDIVIDUAL<br>P. L. Overfelt | 22b. TELEPHONE (*Include Area Code*)<br>619-939-3958<br>22c. OFFICE SYMBOL<br>3814 |


☆ U.S. Government Printing Office: 1986—607-044

CONTENTS



ACKNOWLEDGMENT

The author would like to thank Professor Glen E. Everett of the University of California at Riverside for helpful suggestions.

# INTRODUCTION AND BRIEF HISTORY

The original work on microwave waveguide/cavity discontinuities in the electromagnetic field sense grew out of applications of variational principles (formerly characteristic of quantum mechanics) to electromagnetic theory. This work began during World War II at the Massachusetts Institute of Technology Radiation Laboratories; Marcuvitz (Reference 1) and Schwinger (Reference 2) were responsible for the majority of theoretical developments. They exploited the relationship between electromagnetic boundary value problems and equivalent microwave networks. Theoretical determination of lumped circuit parameters was emphasized that employed variational methods, integral equation methods, equivalent static techniques using conformal mapping (Reference 3), and the transform or Wiener-Hopf technique.

All of the above techniques assume that the terminal plane is far enough away from the discontinuity to consider propagating mode behavior only—the evanescent modes are ignored. If we desire accurate values for the reflection and transmission coefficients of the dominant mode close to the junction or discontinuity plane (or for two or more closely spaced discontinuities), any analysis must include the evanescent modes explicitly.

With the advent of large digital computers, explicit inclusion of evanescent modes became possible, and the first attempts using mode-matching were reported (References 4 through 7). It was assumed that for any junction/discontinuity in a waveguide where the geometrical shape resulted in separable solutions of the Helmholtz equation, the fields in each region could be represented by infinite eigenseries, which were orthogonal and normalized. Using the continuity of tangential electric and magnetic fields over apertures along with $\hat{n} \times \vec{E} = 0$, $\hat{n} \cdot \vec{B} = 0$ for perfectly conducting obstacles, the boundary conditions are formed in terms of products of eigenfunctions and associated constant coefficients, which are the modal reflection and transmission coefficients. These coefficients are evaluated by invoking orthogonality properties of the eigenfunctions and integrating over appropriate parts of the discontinuity plane.

This approach was used by many investigators, not only for metallic but also for surface-wave waveguide discontinuities (Reference 8). However, two major problems exist:

1. The original series that satisfies both the differential equation and the boundary conditions is infinite, and it must remain so if an exact answer is required. Under a very few special circumstances (Reference 7), it is possible

to invert the resulting infinite dimensional matrix to solve the problem; however, in general, this is impossible. Thus, to obtain numerical values of the coefficients, the series must be truncated at some point. No one seemed to know the answer to the question: "How many modes give a sufficiently accurate result?" Finally, Lee, Jones, and Campbell (Reference 9) shed light on this in a very careful treatment of the eigenfunction form of mode-matching and its relationship to an integral equation method. They found that for certain types of waveguide bifurcation problems, the lack of convergence in the solutions was caused by the particular form of mode-matching used and could be removed by using the moment method. However, in the class of iris discontinuity problems, they found difficulties with convergence even when using the moment method.

2. Once a truncation value for the series has been chosen, the ratio between the number of modes in different regions must be considered. This led to the phenomenon of relative convergence (References 4 and 7) in which the coefficients converge to different values depending upon the number of modes taken in each region and the ratio of the modes between regions.

The failure to satisfy the edge condition along the discontinuity plane was thought to cause relative convergence (References 10 and 11). It has been claimed by many that there is a lack of uniqueness in the solutions found from using only continuous tangential fields across a junction. Only when the edge condition is added are we guaranteed to find the one modal ratio that gives the physically correct result. However, as far as we know, this never has been proved mathematically; several investigators have claimed that the modal ratio that causes the system of linear equations to be most "well-conditioned" leads to the correct result (Reference 12).

The least-squares boundary residual method (LSBRM) was proposed to avoid completely the problem of relative convergence (References 13 through 15). Via numerical experimentation, we will show that this method, when combined with traditional mode-matching, converges to the same answer regardless of the modal ratio assumed. This method not only avoids the convergence problem but has several other advantages.

1. The reflection and transmission coefficients can be found separately, thus cutting the size of the matrix to be inverted by half (through partitioning).

2. The matrices to be inverted are Hermitian, thus providing further numerical savings.

3. The technique is characterized by an error function, which must be a minimum when the correct result is obtained.

The LSBRM has one drawback—it converges slowly. Attempts to include a "convergence factor" to speed convergence have not been successful in the sense that no *a priori* way of calculating this factor is known. However, slow

convergence is a small price to pay for a method in which a very stable scattering matrix can be formulated that satisfies the traditional boundary conditions in a least-squares sense.

We have used this technique on two canonical problems: (1) the infinitely thin capacitive iris in a parallel-plate waveguide and (2) the H-plane parallel-plate waveguide step.

Excellent results have been obtained for both. In the following section, the general theory of the LSBRM will be discussed and a scattering matrix formulation (in the least-squares sense) will be developed. The above problems will be discussed in the Canonical Problems section, and results will be shown. (The mathematical details of these two problems are in Appendixes A and B, respectively.) Prior to our conclusions, we will indicate how the relative convergence phenomenon is avoided by the LSBRM.

## GENERAL THEORY

In general, we will consider a junction between two waveguides (cavities) in the following way (see Figure 1). The $a^{(i)}$'s (i = 1,2) are known inputs, and the $b^{(i)}$'s (i = 1,2) are unknown outputs for the junction at z = 0. Using the scattering matrix representation,

$$b = S\,a \tag{1}$$

where b and a are complex column vectors, and S is a complex matrix, and

$$\begin{pmatrix} b^{(1)} \\ \hline b^{(2)} \end{pmatrix} = \left(\begin{array}{c|c} S_{11} & S_{12} \\ \hline S_{21} & S_{22} \end{array}\right) \begin{pmatrix} a^{(1)} \\ \hline a^{(2)} \end{pmatrix} \tag{2}$$

in partitioned form.

The object of the analysis is as follows. We wish to form a scattering matrix [based on mode-matching and least-squares satisfaction of the boundary conditions at the discontinuity (z = 0)] that does not exhibit the relative convergence phenomenon. This is done to solve for the unknown

outputs. We begin with the usual infinite sums of eigenfunctions as tangential electric fields, i.e.,

$$E_{tan}^{(1)} = \sum_{m=1}^{\infty} [a_m^{(1)} e^{-\gamma_m^{(1)} z} + b_m^{(1)} e^{\gamma_m^{(1)} z}] e_m^{(1)} \quad ; \quad z < 0 \tag{3a}$$

$$E_{tan}^{(2)} = \sum_{p=1}^{\infty} [b_p^{(2)} e^{-\gamma_p^{(2)} z} + a_p^{(2)} e^{\gamma_p^{(2)} z}] e_p^{(2)} \quad ; \quad z > 0 \tag{3b}$$

and magnetic fields

$$H_{tan}^{(1)} = \sum_{m=1}^{\infty} [a_m^{(1)} e^{-\gamma_m^{(1)} z} - b_m^{(1)} e^{\gamma_m^{(1)} z}] h_m^{(1)} \quad ; \quad z < 0 \tag{4a}$$

$$H_{tan}^{(2)} = \sum_{p=1}^{\infty} [b_p^{(2)} e^{-\gamma_p^{(2)} z} - a_p^{(2)} e^{\gamma_p^{(2)} z}] h_p^{(2)} \quad ; \quad z > 0 \tag{4b}$$

where $e^{(i)}$ and $h^{(i)}$ (i = 1,2) are the electric and magnetic eigenfunctions, respectively, and $\gamma^{(i)}$ (i = 1,2) is the modal propagation constant along the z-axis (in each region of the guiding structure); m and p represent the number of modes to be used in regions 1 and 2, respectively.

The tangential boundary conditions at z = 0 are

$$E_{tan}^{(1)} = E_{tan}^{(2)} \quad ; \quad 0 < x < b \tag{5a}$$

$$H_{tan}^{(1)} = H_{tan}^{(2)} \quad ; \quad 0 < x < b \tag{5b}$$

$$E_{tan}^{(1)} = 0 \quad ; \quad b < x < a \tag{5c}$$

We must recall also that

$$H_{tan}^{(1)} = J_s \text{ on } z = 0 \ , b < x < a$$

but it is not necessary to include this condition explicitly in order to obtain a unique solution to Equation 1. This and the associated normal boundary conditions will be discussed in the Canonical Problems section and Appendix C.

Using Equations 3 and 4 in 5, the boundary conditions become

$$\sum_{m=1}^{\infty} [a_m^{(1)} + b_m^{(1)}] \, e_m^{(1)} = \sum_{p=1}^{\infty} [b_p^{(2)} + a_p^{(2)}] \, e_p^{(2)} \quad ; \quad 0 < x < b \tag{6a}$$

$$\sum_{m=1}^{\infty} [a_m^{(1)} - b_m^{(1)}] \, h_m^{(1)} = \sum_{p=1}^{\infty} [b_p^{(2)} - a_p^{(2)}] \, h_p^{(2)} \quad ; \quad 0 < x < b \tag{6b}$$

$$\sum_{m=1}^{\infty} [a_m^{(1)} + b_m^{(1)}] \, e_m^{(1)} = 0 \quad ; \quad b < x < a \tag{6c}$$

Arranging the b's on one side and the a's on the other, Equations 6 may be written in matrix form as

$$\begin{pmatrix} e_m^{(1)} & -e_p^{(2)} \\ -h_m^{(1)} & -h_p^{(2)} \\ e_m^{(1)} & 0 \end{pmatrix} \begin{pmatrix} b_m^{(1)} \\ b_p^{(2)} \end{pmatrix} = \begin{pmatrix} -e_m^{(1)} & e_p^{(2)} \\ -h_m^{(1)} & -h_p^{(2)} \\ -e_m^{(1)} & 0 \end{pmatrix} \begin{pmatrix} a_m^{(1)} \\ a_p^{(2)} \end{pmatrix} \tag{7}$$

This leads to a matrix equation of the abstract form

$$L \, b = M \, a \tag{8}$$

Many investigators (References 5 through 7) simply assumed that by applying the orthogonality properties of the eigenfunctions and integrating all boundary conditions over the appropriate cross section at z = 0 the unknown outputs are given by

$$b = \int_c (L^{-1} M dc)\, a \tag{9}$$

and thus

$$S = \int_c L^{-1} M\, dc \tag{10}$$

is the scattering matrix of the problem in Figure 1. While this is quite true in a formal sense, this course leads to numerical difficulties. The scattering matrix in Equation 10 exhibits the relative convergence phenomenon (see the Introduction and Brief History section) and is unsuitable for direct numerical solution of the unknown outputs.

By satisfying the boundary conditions in a least-squares sense, one avoids the relative convergence problem. In terms of the scattering matrix, we use the fact that the adjoint (complex conjugate transpose) of the L matrix can be multiplied through from the left on each side of Equation 8. Thus, from Equation 8,

$$L^t L\, b = L^t M\, a \tag{11}$$

Integrating $L^tL$ and $L^tM$ over the appropriate parts of the boundary at z = 0 results in

$$S = H^{-1} f \tag{12}$$

where $H = \int_C L^tL\ dc$ is square and Hermitian, and $f = \int_C L^tM\ dc$ is the known integrated input (sometimes called the forcing function). Of course, the scattering matrix of Equation 12 reduces formally to that of Equation 10, but Equation 12 is numerically stable. The scattering matrix of Equation 12 is guaranteed to converge to a given result as the number of modes in either region is increased. The scattering matrix in Equation 10 will converge to different answers depending upon the number of modes used and the modal ratio r = m/p as m and p are increased (Reference 4).

The error associated with this least-squares scattering matrix is found from Equation 1. The "distance" between two complex quantities in a physical sense (References 16 and 17) is determined by

$$d(f,g) = |f - g| \tag{13}$$

Thus,

$$\varepsilon = |b - Sa| \tag{14}$$

gives a physically meaningful indication of how far away (i.e., when m and p approach infinity) any truncated result is from the exact answer. Thus,

$$\varepsilon = (b^t - a^t S^t)\,(b - Sa)$$

$$= b^t b - b^t S a - a^t S^t b + a^t S^t S a \tag{15}$$

If the boundary conditions are perfectly matched, the error $\varepsilon$ is zero. It may not be possible to have $\varepsilon = 0$ exactly except when the number of modes taken on either side of the junction is allowed to approach infinity. Since truncation is a numerical necessity, the set of unknown outputs [i.e., $b_m^{(1)}$ and $b_p^{(2)}$] that causes the error to be a minimum is the physically correct set (References 18 and 19).

## CANONICAL PROBLEMS

We depart from the theory of the General Theory section to discuss two particular waveguide discontinuities: (1) the infinitely thin capacitive iris in a parallel-plate waveguide and (2) the asymmetrical H-plane parallel-plate waveguide step. The above were chosen as test cases for a number of reasons: (a) Both are *two-dimensional—this means there will be fewer nonzero field* components to match across the discontinuities; (b) both have been done before by other methods so that comparison values exist; and (c) (1) and (2) are in different problem classes and thus provide a fair test of the LSBRM.

The details of deriving the H matrices that must be inverted to compute the reflection and transmission coefficients for (1) and (2) are given in Appendixes A and B, respectively.

In the capacitive iris problem (see Figure A-1), we have a number of conditions that ensure the validity of the solution. First of all, each of the tangential boundary conditions must be satisfied by the computed coefficients, i.e., Equations A-7 must be satisfied simultaneously. Thus, the tangential electric fields on either side of the iris from $b < y < a$ must go to 0 and be continuous from $0 < y < b$.

Consider Figure 2, where the waveguide height, a, is 1.2 centimeters and the iris has a length $b = a/2 = 0.6$ centimeter at a frequency of 10 gigahertz ($\lambda_0 = 3$ centimeters). This is a plot of the normalized tangential electric field magnitudes in regions 1 and 2 [i.e., $|E_y^{(1)}|$ and $|E_y^{(2)}|$] as functions of the guide height along the discontinuity plane at $z = 0$. It is clear that using 26 modes in each region, i.e., $M = N = 26$, gives virtually identical fields across the aperture and causes the fields to drop sharply to 0 at $y = b = 0.6$ on the perfectly conducting iris. The real and imaginary parts of the dominant transverse electromagnetic (TEM) mode reflection and transmission coefficients are given as well as the normalized susceptance $B/Y_0$ of the associated equivalent circuit. The two problems with Figure 2 are that the fields are not 0 at exactly $y = 0.6$, and $B/Y_0 = 1.725$, which is in error by 8.5%. By taking a larger number of modes, we can correct these problems. For 76 modes on each side with all other parameters the same as in Figure 2, the fields fall to exactly 0 at $y = 0.6$ and the normalized susceptance is in error by only 3.8%, as shown in Figure 3.

Similarly, the tangential magnetic fields must be continuous in the aperture and differ from each other by the current density on the iris. Looking at Figures 4 and 5, we see that this is true. Figure 4 compares the tangential magnetic-field magnitudes for 26 modes on each side of the iris. In Figure 5 with 76 modes in each region, the fields match better, particularly at the edge of the iris ($y = 0.6$), and the fields in the aperture are tending toward 0 as the number of modes increases. By symmetry, we know that $|H_x^{(1)}| = |H_x^{(2)}| = 0$ for $0 < y < b$ if the boundary conditions are matched exactly. Thus, for increasing mode number, we note that it is more difficult to match the tangential magnetic fields over the discontinuity plane than the tangential electric fields, and further experimentation shows that this is always true. This may be a consequence of the fact that the tangential boundary conditions on the magnetic fields over the perfectly conducting portion of the discontinuity [i.e., $\hat{n} \times (\vec{H}^{(1)} - \vec{H}^{(2)}) = \vec{J}_S$] are not explicitly used in the original formulation of the scattering matrix.

Now that the tangential boundary conditions have been satisfied, we must check that normal conditions are also satisfied, although this is usually taken for granted. In this problem, since the iris generates only higher order transverse magnetic (TM) modes, the only nonzero normal field component to the boundary at $z = 0$ is $E_z$. We know that continuous normal $\vec{B}$ and $\vec{D}$ are the normal conditions to be satisfied across the aperture; therefore, on $0 < y < b$, $E_z^{(1)} = E_z^{(2)}$. Looking at Figures 6 and 7, we see that this is indeed true for 26 and 76 modes in each region, respectively. In fact, using $\nabla \cdot \vec{D} = 0$ and the

continuity equation, $E_z^{(1)} = E_z^{(2)}$ for $0 < y < a$ and, thus, continuous normal $\bar{D}$ is true along the entire discontinuity plane.

The third condition to be met is that for $a = 0.4\ \lambda$ and $b = a/2$, the normalized susceptance across the junction is $B/Y_0 = 1.59$. From Figure 8, we see that as the number of modes is increased, the susceptance is tending toward this value for a modal ratio, M/N = 1. At 75 modes on each side, the susceptance value is 1.65, which is ~ 3.8% error as compared with the exact value.

As we mentioned in the General Theory section, the error function can be computed from Equation 15 when the coefficients are known. This error must be a minimum for a given set of modes, and we want it to tend to 0 as the number of modes increases. From Figure 9 for a modal ratio of 1, we see that the error function for the reflection and transmission coefficients (i.e., the b's) is less than 5% after only 8 or 10 modes on each side, and it decreases toward 0 in a smooth, well-behaved manner.

In order to compare the theoretical model with experiment, the quantities of interest are the magnitude and phase of the dominant mode reflection and transmission coefficients. Figure 10 shows the magnitude of the reflection and transmission coefficients as functions of increasing mode number for a modal ratio of 1. Figure 11 shows the phases as functions of increasing mode number. After 20 or 25 modes, both quantities are changing only slightly with increasing mode number. These two plots confirm the results of the error function in Figure 9. For practical purposes, it is necessary to take only 10 or 15 modes on each side of the discontinuity to obtain less than 5% accuracy in the dominant mode reflection and transmission coefficient values. It is also of interest to compute the reflection and transmission coefficients over a frequency band. Figures 12 and 13 show the reflection and transmission coefficient magnitudes and phases, respectively, at X-band. Over the frequency range shown, the reflection coefficient magnitude increases with increase in frequency, whereas the transmission magnitude decreases. The phases of both coefficients remain relatively constant over this range.

Finally, although we have shown that the numerical results all converge as the number of modes increases, we must also show convergence with respect to the modal ratio. So far the modal ratios in all cases have been 1. But consider how the normalized susceptance is affected by the modal ratio. In Figure 8, where the ratio is 1 at 25 modes on each side, the susceptance is about 1.725. In Figure 14, where the ratio is 2 for 50 modes in region 1 and 25 modes in region 2, $B/Y_0 = 1.735$. In Figure 15, where the ratio is 3 for 75 modes in region 1 and 25 modes in region 2, $B/Y_0 = 1.74$. Obviously, while the susceptance is tending to the correct answer regardless of modal ratio, a poorly chosen ratio will cause a much larger number of total modes to be used in order to achieve a particular accuracy. In this problem, since the waveguide is the same height on either side on the iris, intuition indicates that an equal number of modes in each region is the "best" ratio. More will be said

concerning this aspect of the analysis for the H-plane parallel plate step problem.

Thus, after considering all of the above checks on the capacitive iris solution, we can conclude that the LSBRM is numerically stable, accurate to less than 5% (depending on the number of modes one wishes to take), and is slowly convergent, although the convergence appears to be guaranteed.

In the asymmetrical H-plane parallel-plate waveguide problem (details in Appendix B), the situation is a little more complex (see Figure B-1). Again, we (at $z = 0$) have our aperture between $0 < x < b$ and a perfectly conducting surface between $b < x < a$. For $TE_{01}$ mode incidence, the step generates only higher order TE modes and, thus, $H_z$, $H_x$, and $E_y$ are the only nonzero field components. The tangential boundary conditions on $z = 0$ that are used in formulating the H-matrix are

$$E_y^{(1)} = 0 \quad ; \quad b < x < a \tag{16a}$$

$$H_x^{(1)} = H_x^{(2)} \quad ; \quad 0 < x < b \tag{16b}$$

$$E_y^{(1)} = E_y^{(2)} \quad ; \quad 0 < x < b \tag{16c}$$

An auxiliary condition not explicitly included is the tangential magnetic field condition on the step. (For further discussion of boundary conditions, see Appendix C.)

$$H_x^{(1)} = H_{tan}^{(1)} = J_s \quad ; \quad b < x < a \tag{17}$$

[We assume that $\vec{H}^{(2)}$ and $\vec{E}^{(2)}$ no longer exist in region 2 when $x > b$, since that region is bounded by perfect conductors.]

The normal conditions on $z = 0$ are

$$H_z^{(1)} = H_z^{(2)} \quad ; \quad 0 < x < b \tag{18a}$$

$$H_z^{(1)} = 0 \quad ; \quad b < x < a \tag{18b}$$

Not only must all of the above be satisfied, but the error function must be a minimum as before.

To show that the previous conditions are all satisfied, we use Figure B-1 and let (1) the larger guide height, a, be 2.7 centimeters, (2) the smaller guide height, b, be 2 centimeters, and (3) the frequency be 10 gigahertz. M and N refer to the maximum number of modes used in the large and small guides, respectively. Figures 16 and 17 are plots of the electric field magnitudes as functions of waveguide height along the step at z = 0. Figure 16 shows how well the fields match for 20 modes in each region, while Figure 17 shows the match for 50 modes in each region. For 50 modes, the tangential electric field boundary condition is satisfied almost exactly.

The tangential magnetic field magnitudes as functions of the guide height along z = 0 are shown in Figures 18 and 19. As for the capacitive iris problem, the tangential magnetic fields are more difficult to match than the tangential electric fields. In Figure 18, $|H_x^{(1)}|$ and $|H_x^{(2)}|$ are fairly well matched for 20 modes until close to the discontinuity, where $|H_x^{(2)}|$ goes to 0 (it no longer exists), but $H_x^{(1)} = J_s$. In Figure 19, the fields match better for 50 modes in each region; however, there is still some discrepancy close to the discontinuity.

The only normal condition is continuous normal $\vec{B}$ (or $\vec{H}$, in this case) on $0 < x < b$, and $H_z^{(1)} = 0$, as shown above, on $b < x < a$. Figures 20 and 21 are plots of the normal magnetic field magnitudes as functions of the guide height at z = 0. For 20 modes in each region (Figure 20), the field match is poor in both the aperture region and the step region. Not until we increase the number of modes in each region to 75 (Figure 21), do the normal fields match well.

Figure 22 is a plot of the error function versus mode number for a modal ratio of 1. Since the step in this example is not very large, it is necessary to take only 7 or 8 modes to obtain an accuracy of less than 4% in the computed reflection and transmission coefficients. The dominant mode reflection coefficient magnitude as a function of mode number is shown in Figure 23. This plot supports the results of the error function, i.e., only 7 or 8 modes need to be included to give accurate values of reflection.

Now consider the example where a = 2.7 but b ~ a/2 = 1.4 at 10 gigahertz. This is a much larger step than in the previous example, and it will serve to illustrate an interesting effect concerning the modal ratio. Consider Figures 24 through 26. If the total number of modes, P = M + N, is 100, then Figures 24, 25, and 26 show the error as a function of increasing mode number for modal ratios 1, 2, and 3, respectively (i.e., M = 50, N = 50; M = 66, N = 33; and M = 75, N = 25). The geometric ratio for the waveguide heights is a/b ~ 2. We would like to find the smallest possible error for a given value of P. By comparing Figures 24 through 26, it is clear that a modal ratio of 2 gives the smallest error when P = 100. Also, we would like to find the smallest possible error for the smallest number of total modes P. For example, M = 50, N = 50 gives an error of 3.83%, whereas M = 50, N = 25 gives an error of 3.96%. An increase in accuracy of 0.13% is not worth the extra computation needed to include 25 extra modes. We see that the modal ratio is controlled in some sense by the geometric ratio, a/b,

and in general we can confirm the known result that if $a/b \sim 2$, then $m/n \sim 2$ is the "best" modal ratio both in terms of the error and the total number of modes P.

## CONCLUSIONS

We have used the least-squares boundary residual method (LSBRM) to obtain very accurate numerical values for the modal reflection and transmission coefficients, the electric and magnetic field components, and the error associated with certain types of waveguide discontinuity problems. We have considered the general theory in terms of a scattering matrix representation and have shown that the theory works very well for two canonical problems: (1) the thin capacitive iris in a parallel-plate waveguide and (2) the asymmetrical H-plane parallel-plate waveguide step. The method exhibits slow convergence for large discontinuties; however, its advantages—explicit evanescent modes, guaranteed convergence, excellent accuracy, and an associated error function, which must be a minimum for the physically correct solution—are significant.

In the immediate future, we will continue to look at similar discontinuity problems but with the following modifications:

1. Discontinuities in cavities with perfectly conducting end plates
2. Discontinuities in cylindrical and spherical geometries
3. Discontinuities that generate both transverse electric and transverse magnetic higher order modes
4. Multiple discontinuities less than a wavelength apart

This is a very powerful and versatile technique for predicting the scattering properties of any discontinuity or junction, provided the geometry can be represented in terms of eigenseries. It will enhance our capability to model complex microwave devices so that their scattering properties can be well understood.

## FIGURES

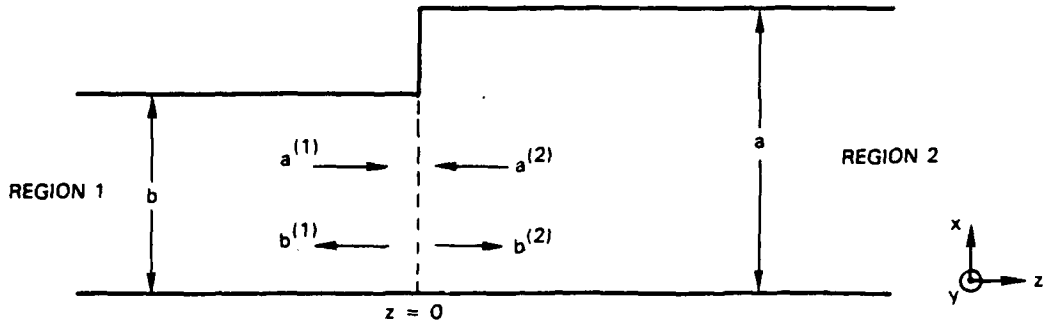


FIGURE 1. Geometry for Junction Between Two General Waveguides.

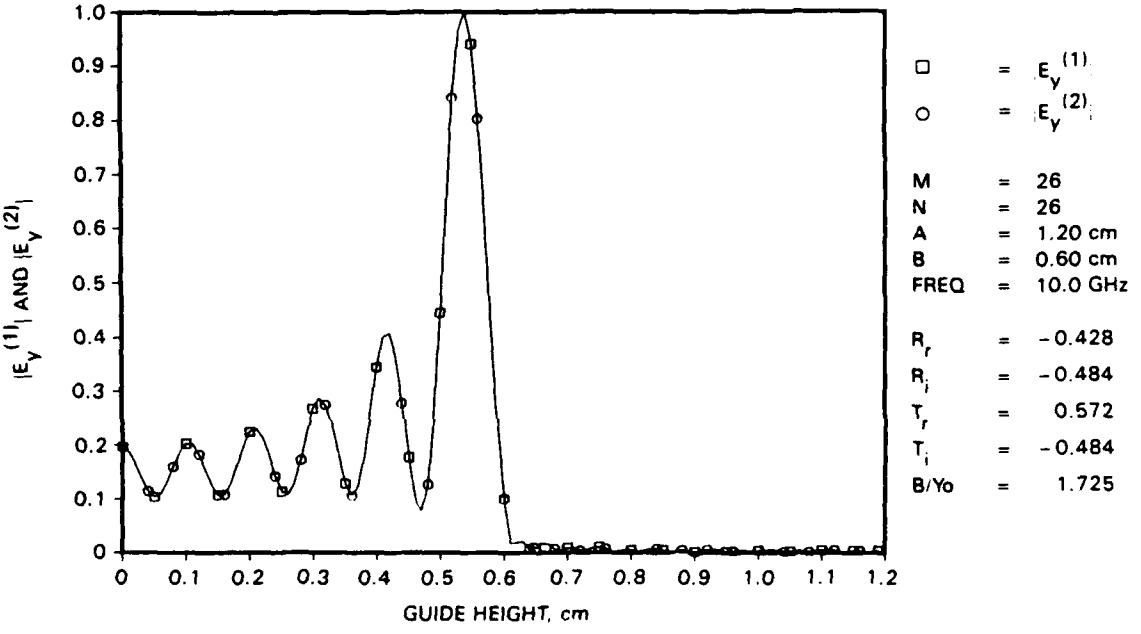


FIGURE 2. Normalized Tangential Electric Field Magnitudes Versus Guide Height for Capacitive Iris Junction (26 Modes).

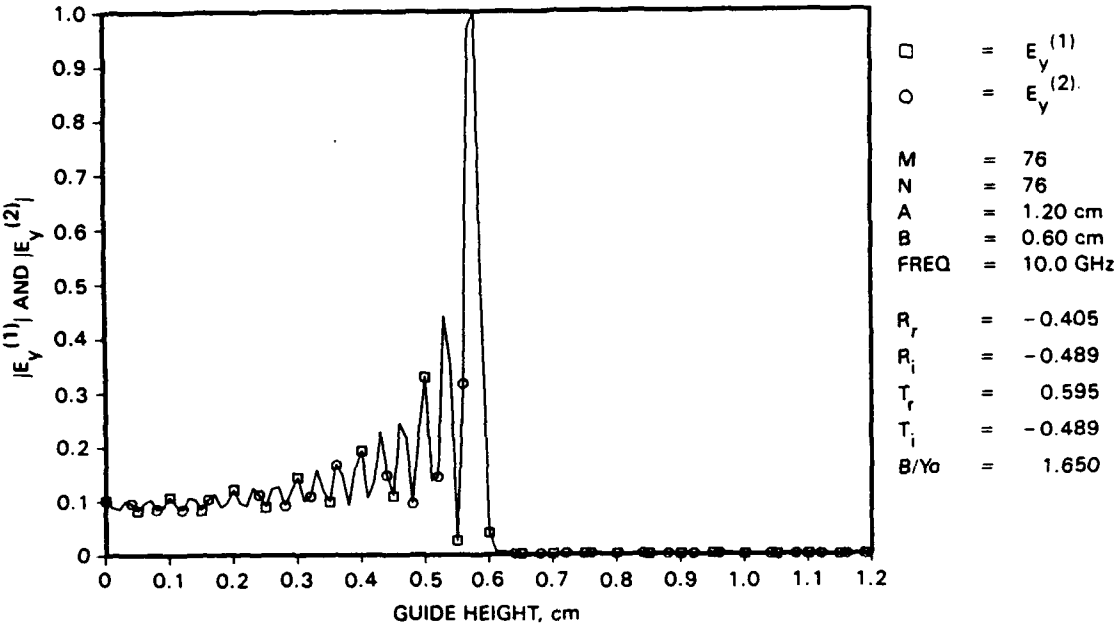


FIGURE 3. Normalized Tangential Electric Field Magnitudes Versus Guide Height for Capacitive Iris Junction (76 Modes).

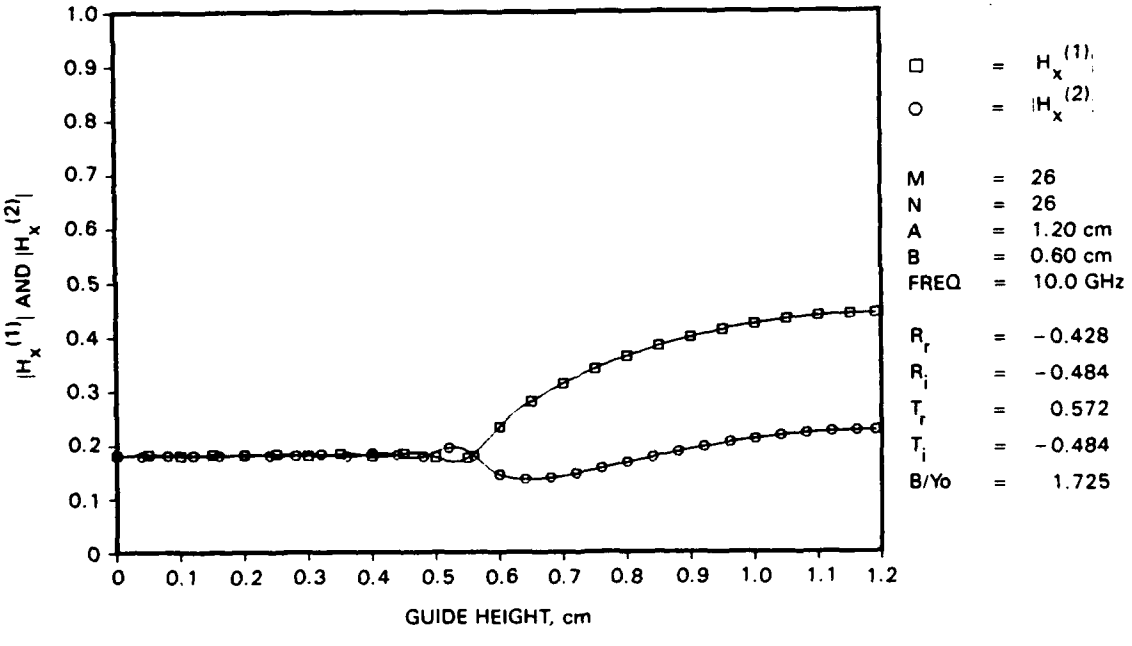


FIGURE 4. Normalized Tangential Magnetic Field Magnitudes Versus Guide Height for Capacitive Iris Junction (26 Modes).

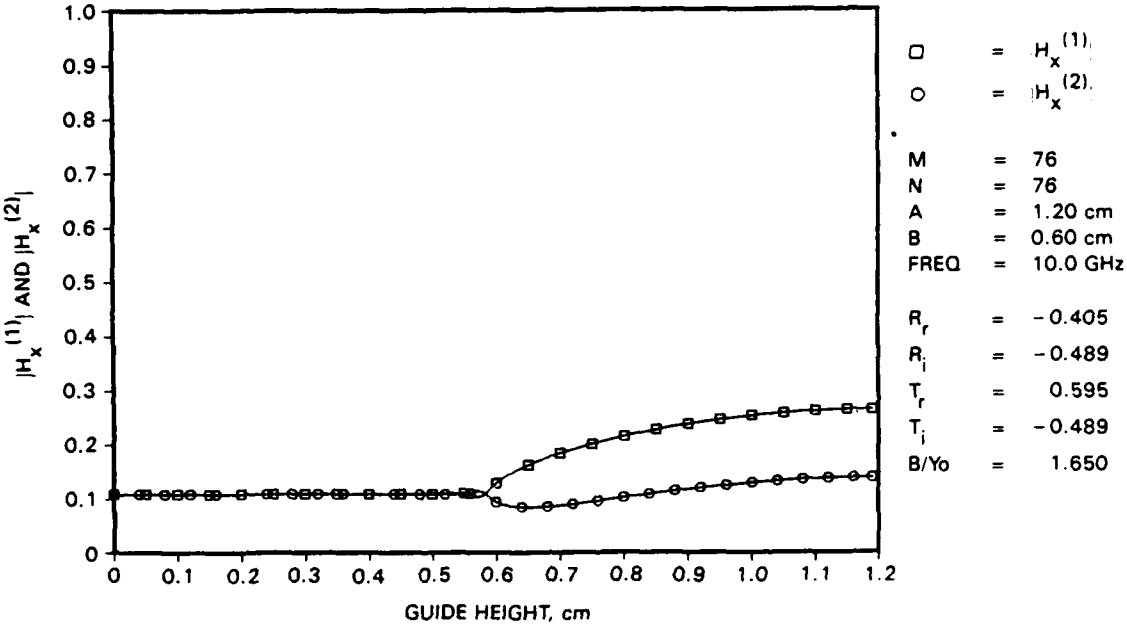


FIGURE 5. Normalized Tangential Magnetic Field Magnitudes Versus Guide Height for Capacitive Iris Junction (76 Modes).

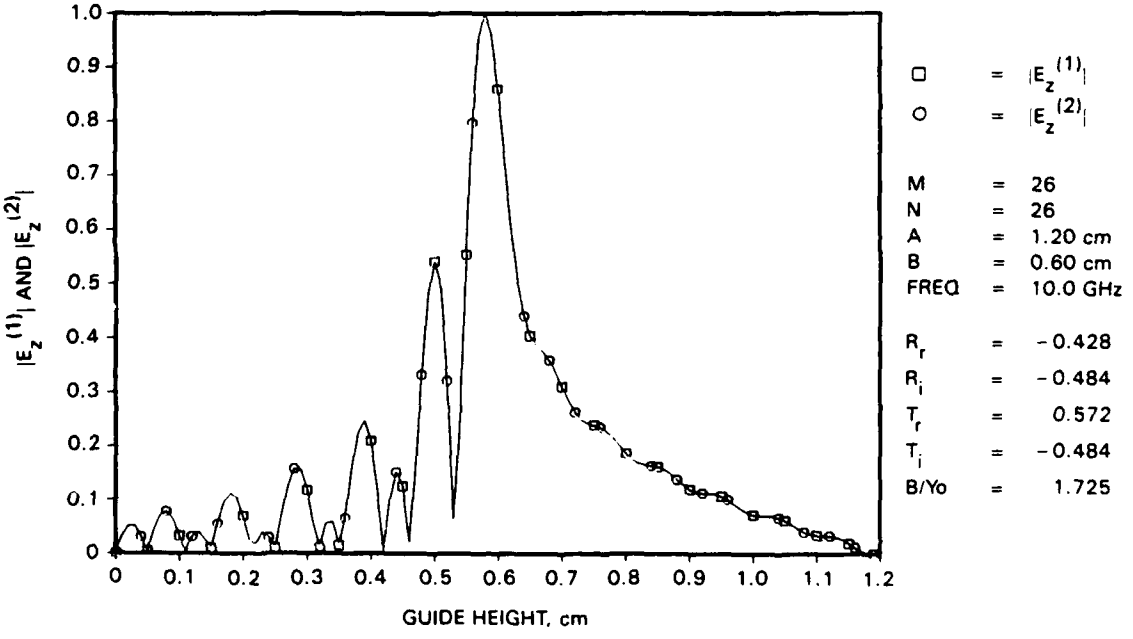


FIGURE 6. Normalized Normal Electric Field Magnitudes Versus Guide Height for Capacitive Iris Junction (26 Modes).

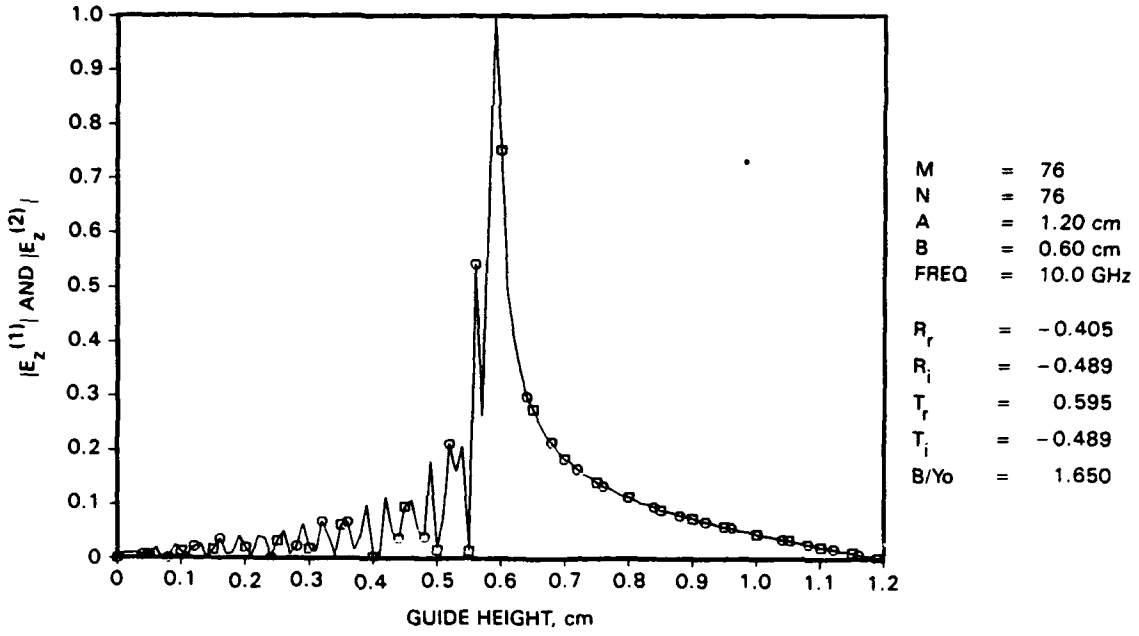


FIGURE 7. Normalized Normal Electric Field Magnitudes Versus Guide Height for Capacitive Iris Junction (76 Modes).

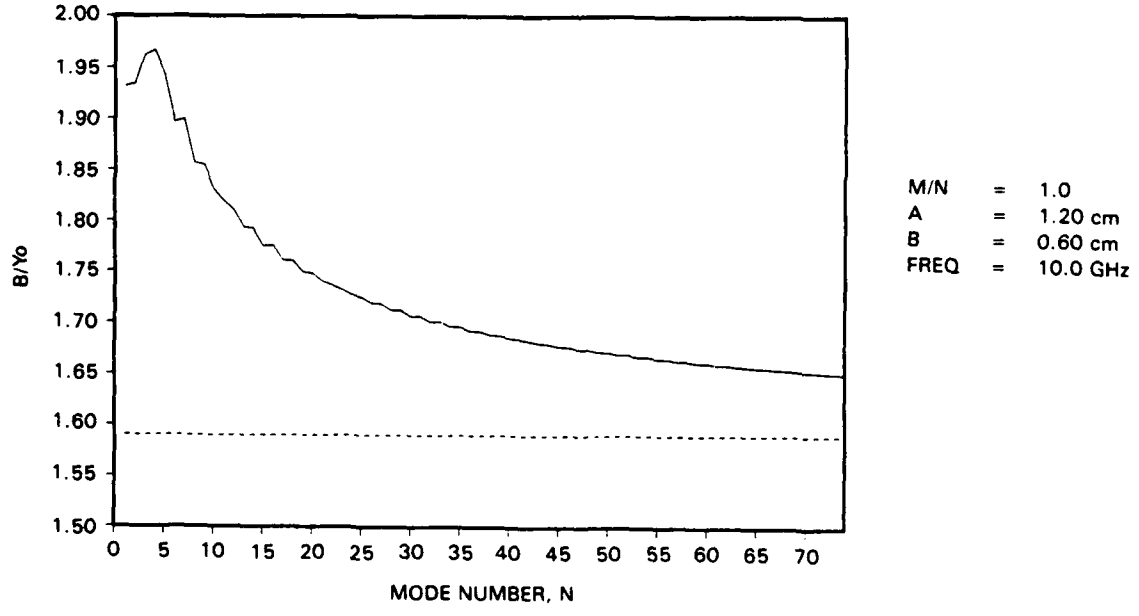


FIGURE 8. Normalized Susceptance Versus Mode Number for Capacitive Iris Junction (Modal Ratio of 1).

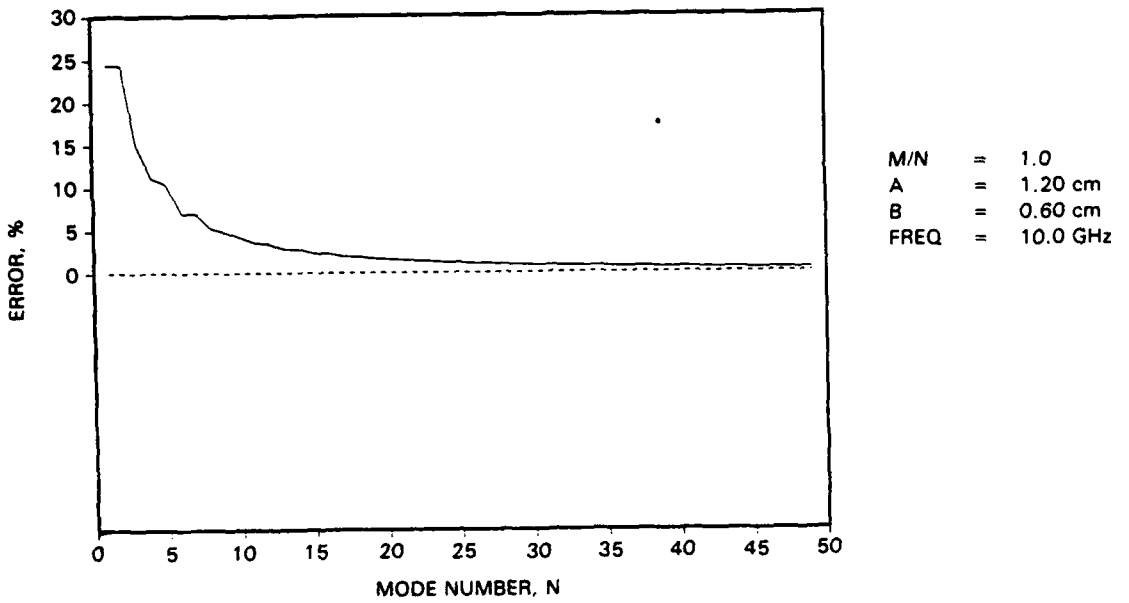


FIGURE 9. Error Versus Mode Number for Capacitive Iris Junction (Modal Ratio of 1).

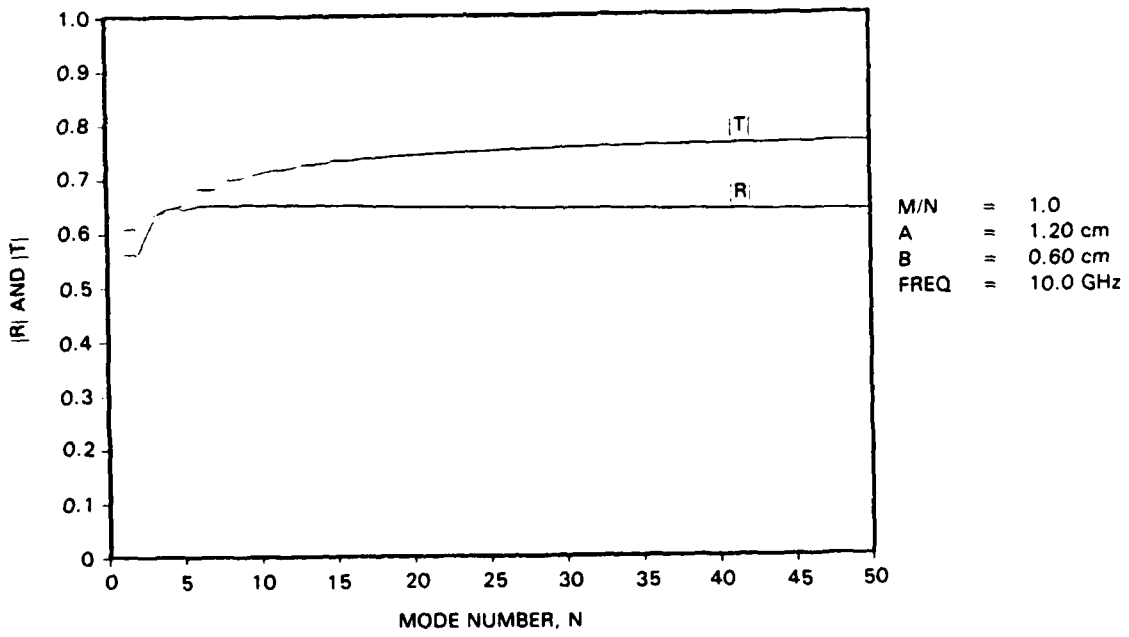


FIGURE 10. TEM Mode Reflection and Transmission Magnitude Versus Mode Number for Capacitive Iris Junction.

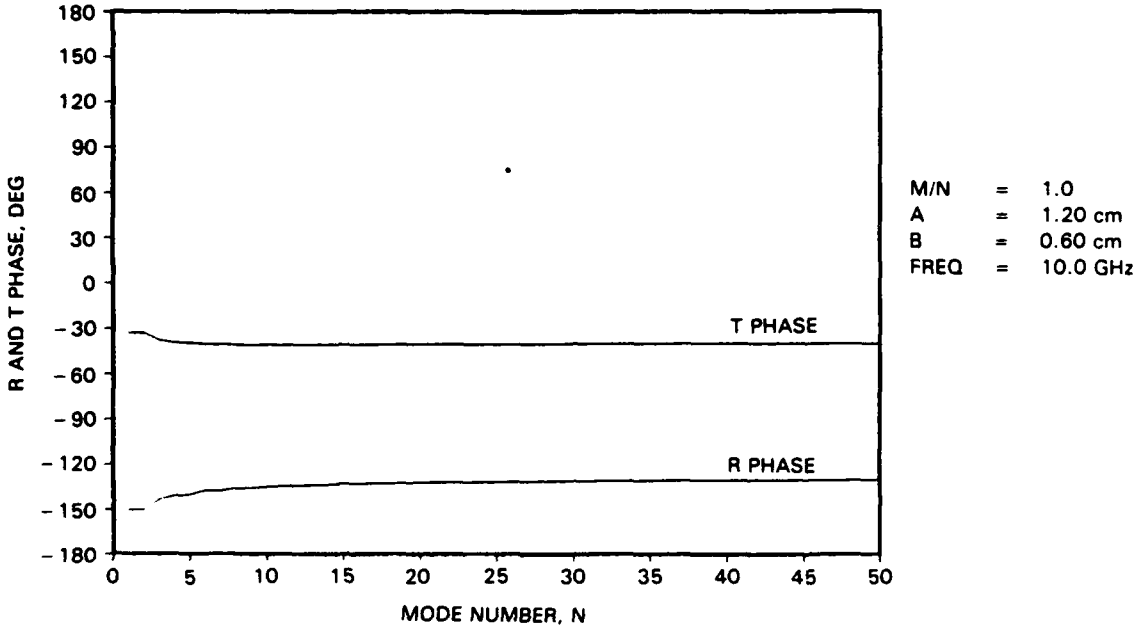


FIGURE 11. TEM Mode Reflection and Transmission Phase Versus Mode Number for Capacitive Iris Junction.

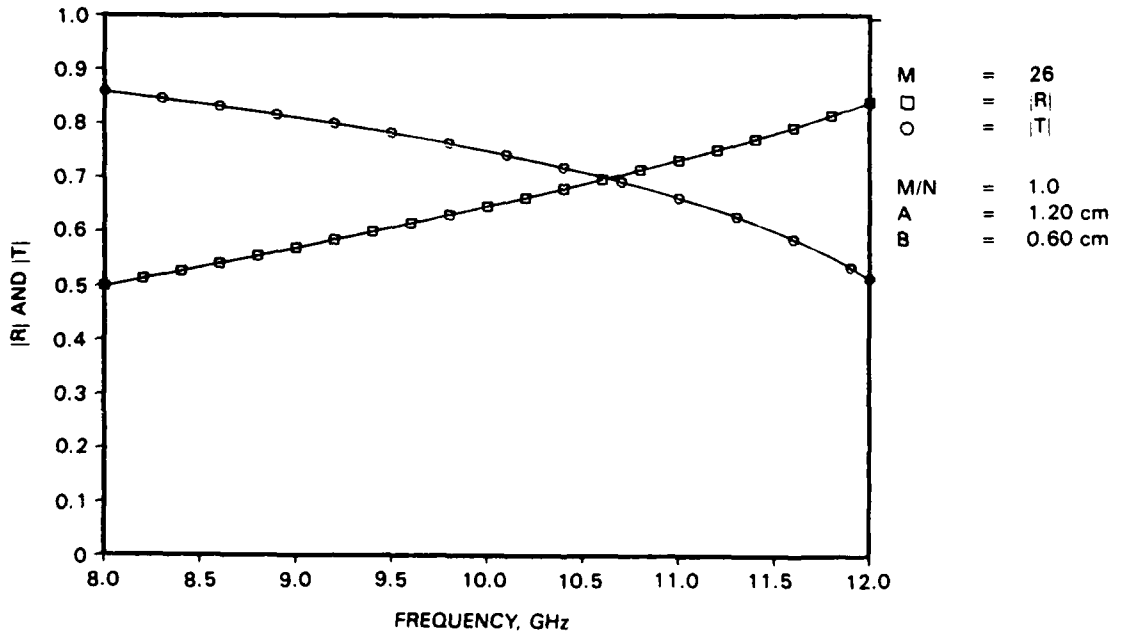


FIGURE 12. TEM Mode Reflection and Transmission Magnitude Versus Frequency for Capacitive Iris Junction.

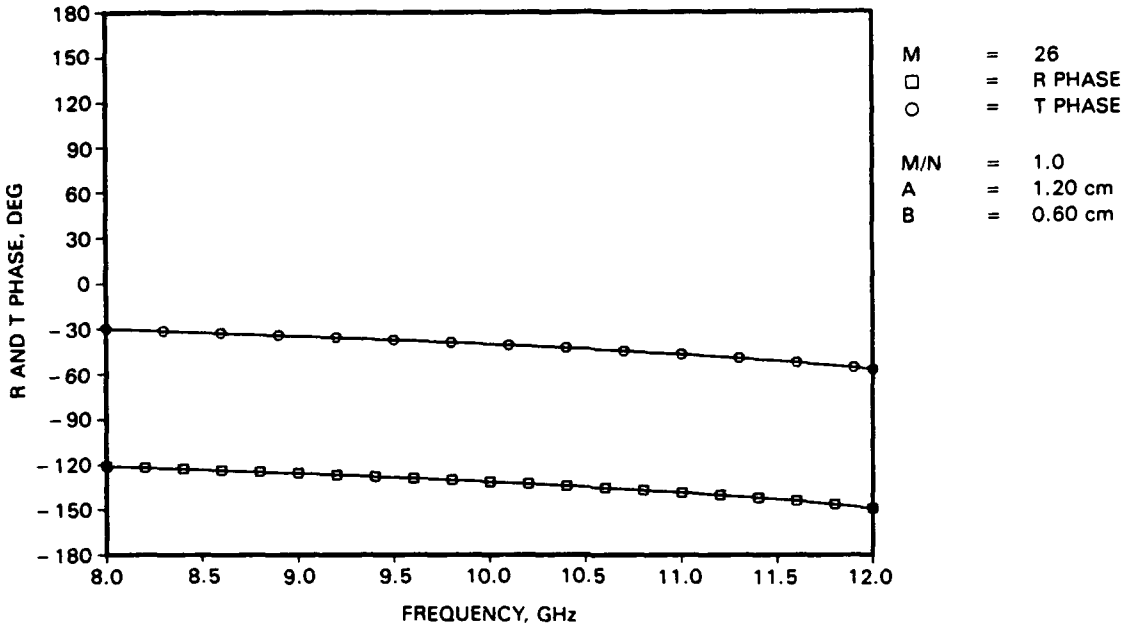


FIGURE 13. TEM Mode Reflection and Transmission Phase Versus Frequency for Capacitive Iris Junction.

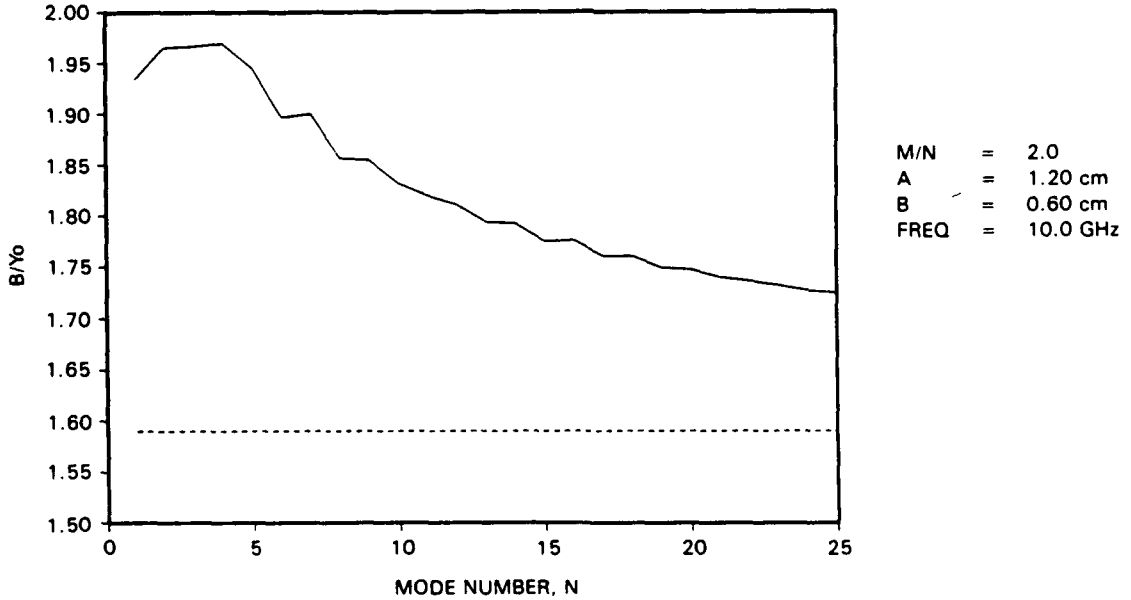


FIGURE 14. Normalized Susceptance Versus Mode Number for Capacitive Iris Junction (Modal Ratio of 2).

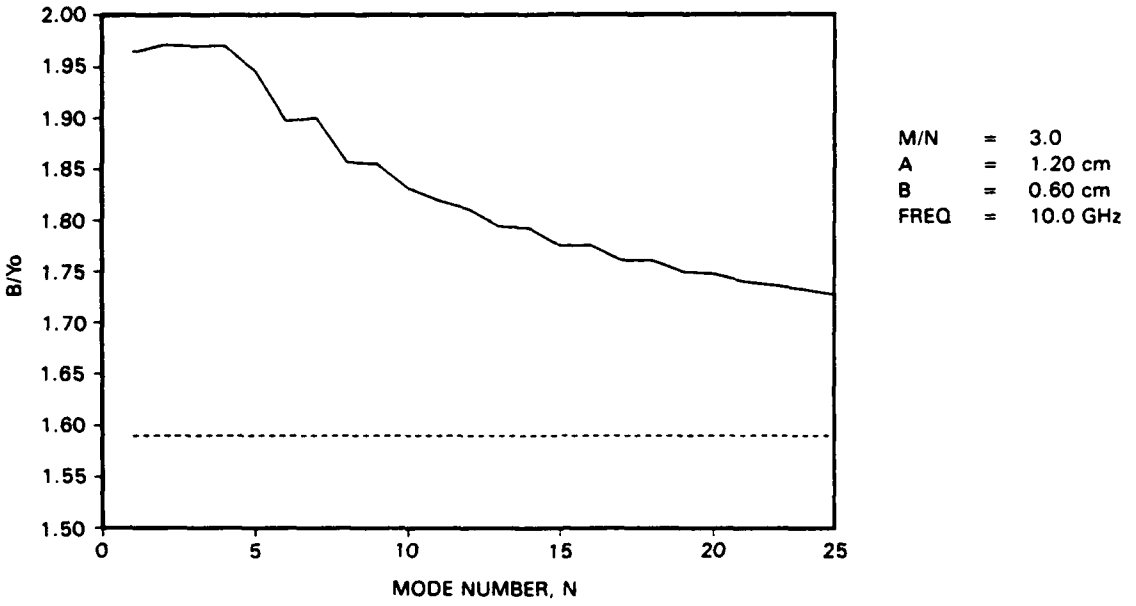


FIGURE 15. Normalized Susceptance Versus Mode Number for Capacitive Iris Junction (Modal Ratio of 3).

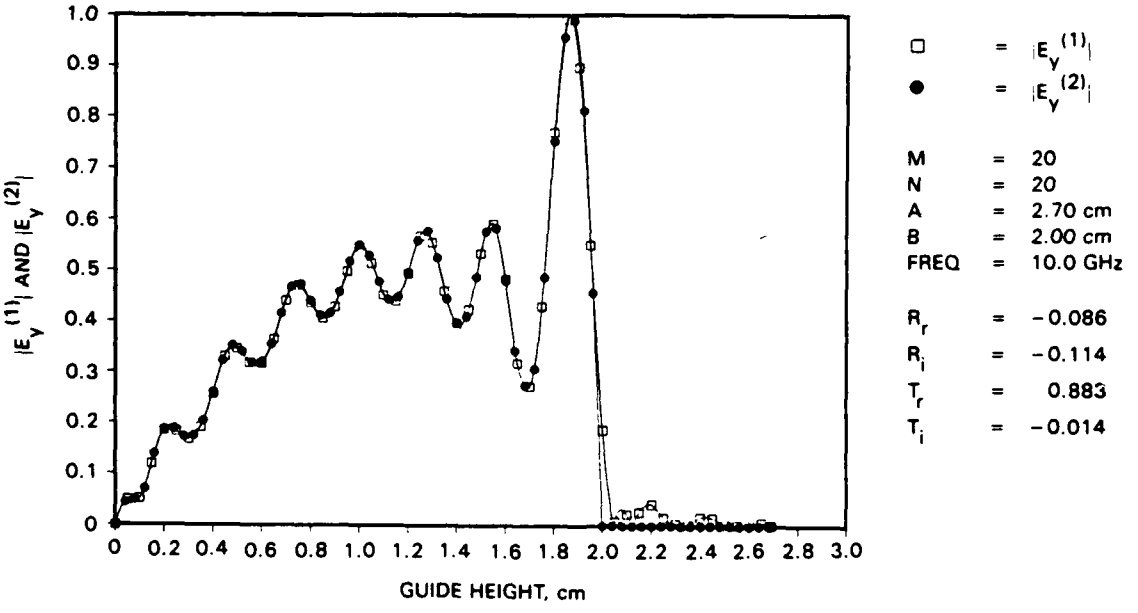


FIGURE 16. Normalized Tangential Electric Field Magnitudes Versus Guide Height for Parallel-Plate Waveguide Junction ($TE_{01}$ Mode Incidence From Larger Guide, 20 Modes).

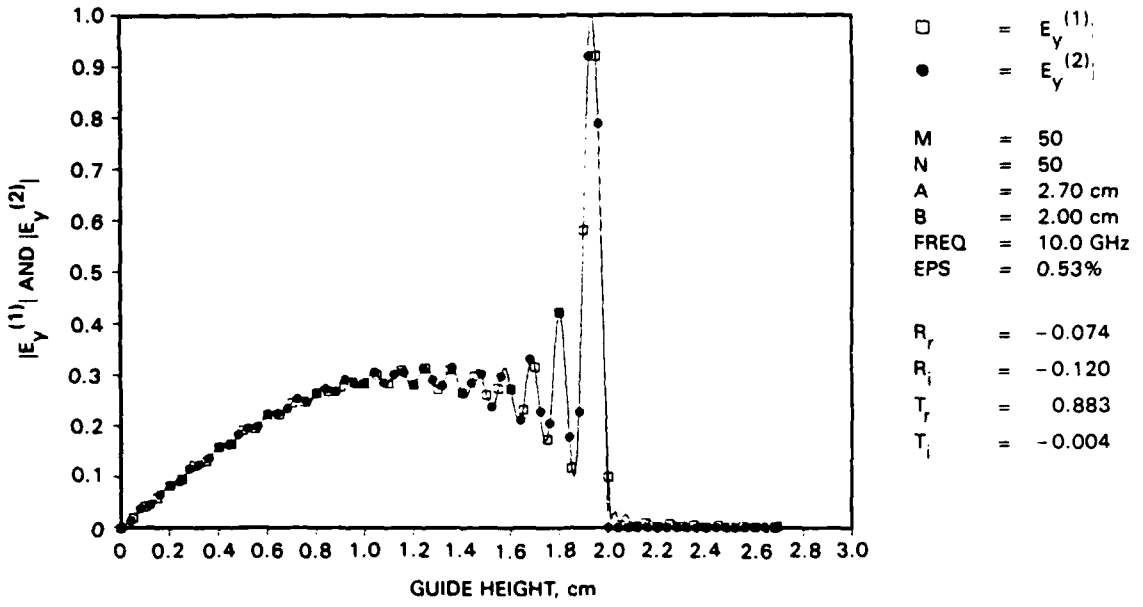


FIGURE 17. Normalized Tangential Electric Field Magnitudes Versus Guide Height for Parallel-Plate Waveguide Junction ($TE_{01}$ Mode Incidence From Larger Guide, 50 Modes).

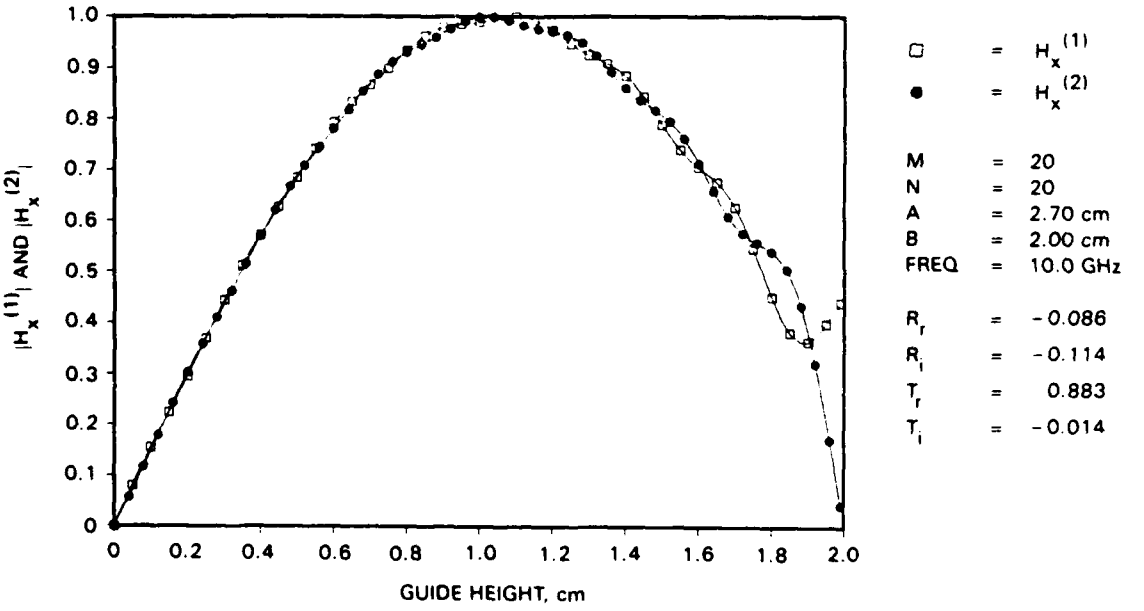


FIGURE 18. Normalized Tangential Magnetic Field Magnitudes Versus Guide Height for Parallel-Plate Waveguide Junction ($TE_{01}$ Mode Incidence From Larger Guide, 20 Modes).

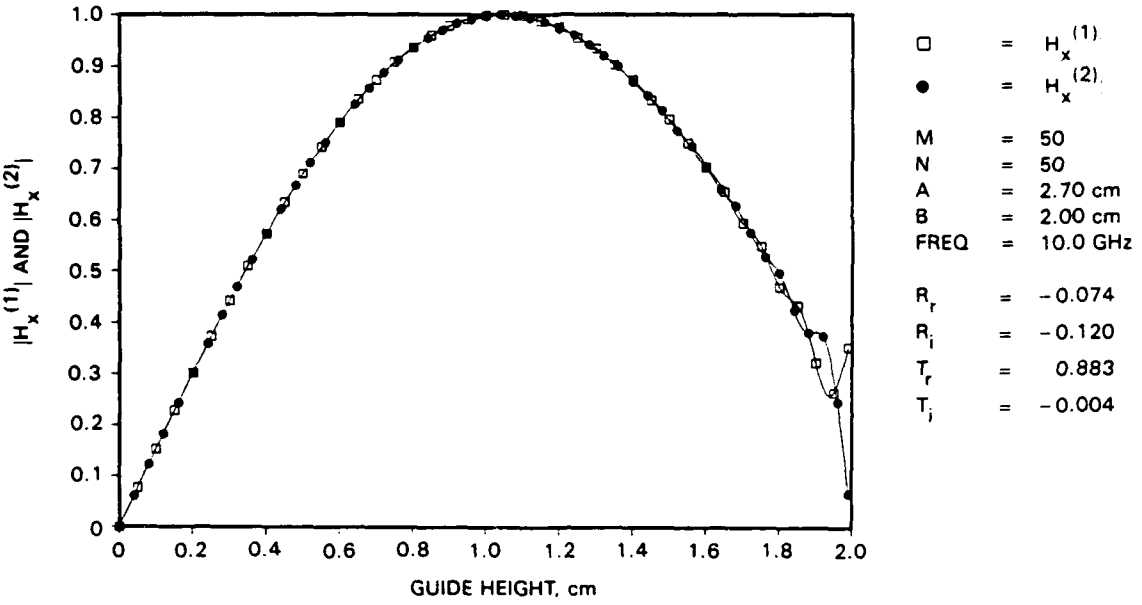


FIGURE 19. Normalized Tangential Magnetic Field Magnitudes Versus Guide Height for Parallel-Plate Waveguide Junction ($TE_{01}$ Mode Incidence From Larger Guide, 50 Modes).

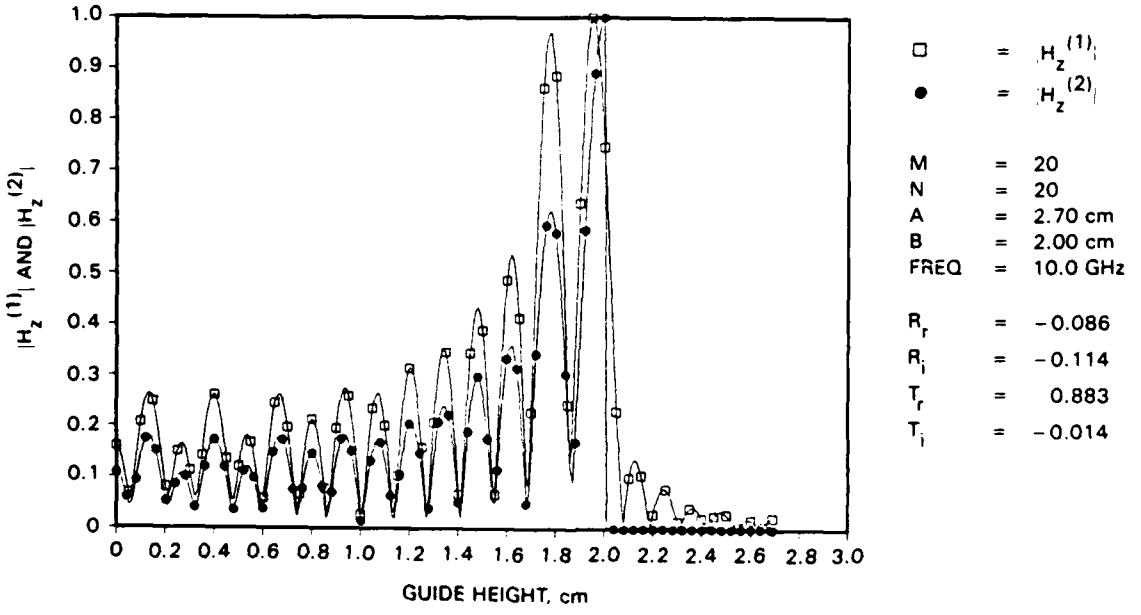


FIGURE 20. Normalized Normal Magnetic Field Magnitudes Versus Guide Height for Parallel-Plate Waveguide Junction ($TE_{01}$ Mode Incidence From Larger Guide, 20 Modes).

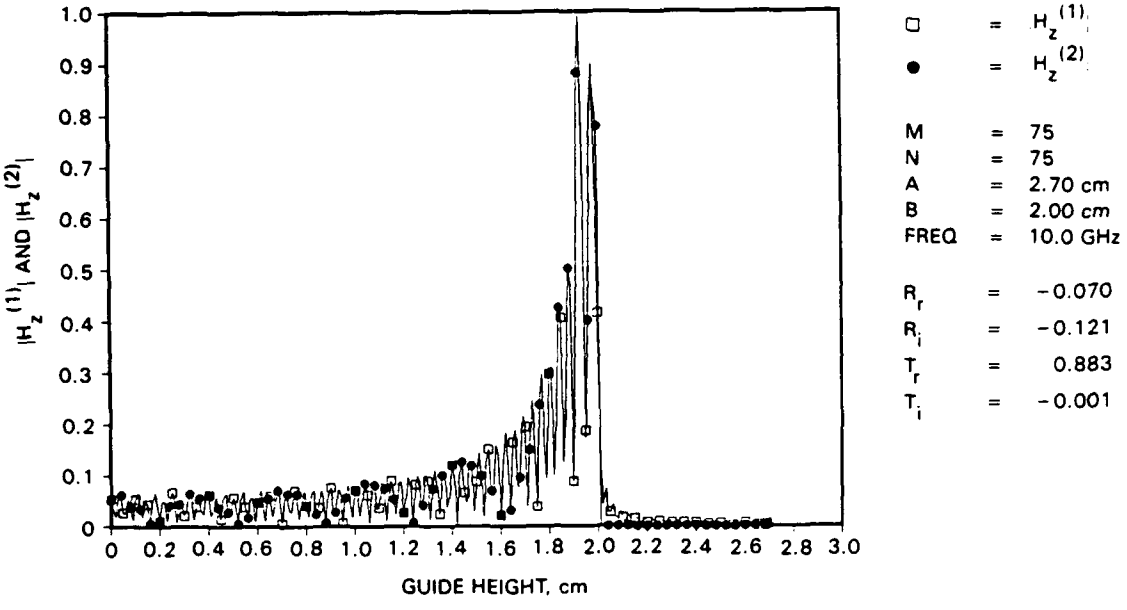


FIGURE 21. Normalized Normal Magnetic Field Magnitudes Versus Guide Height for Parallel-Plate Waveguide Junction ($TE_{01}$ Mode Incidence From Larger Guide, 75 Modes).

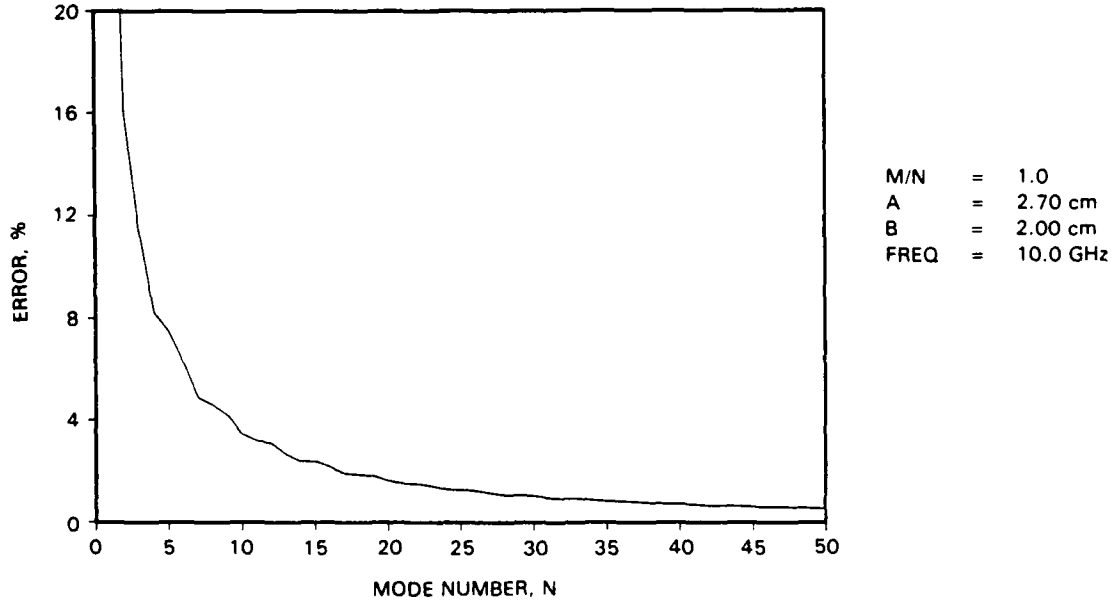


FIGURE 22. Error Versus Mode Number for Parallel-Plate Waveguide Junction ($TE_{01}$ Mode Incidence, Modal Ratio of 1).

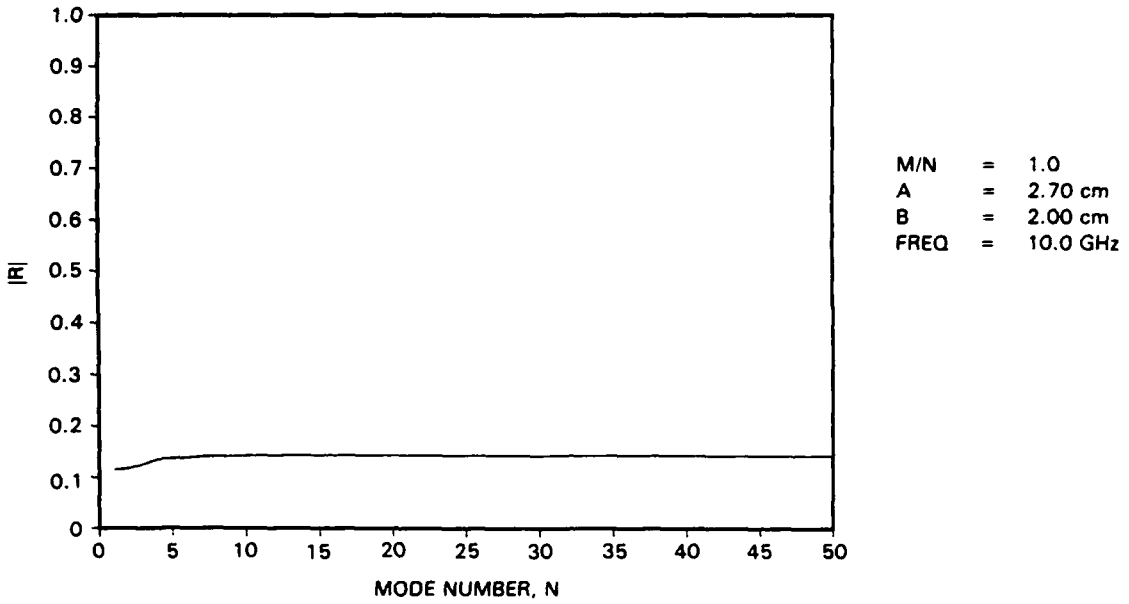


FIGURE 23. Reflection $TE_{01}$ Mode Coefficient Magnitude Versus Mode Number for Parallel-Plate Waveguide Junction.

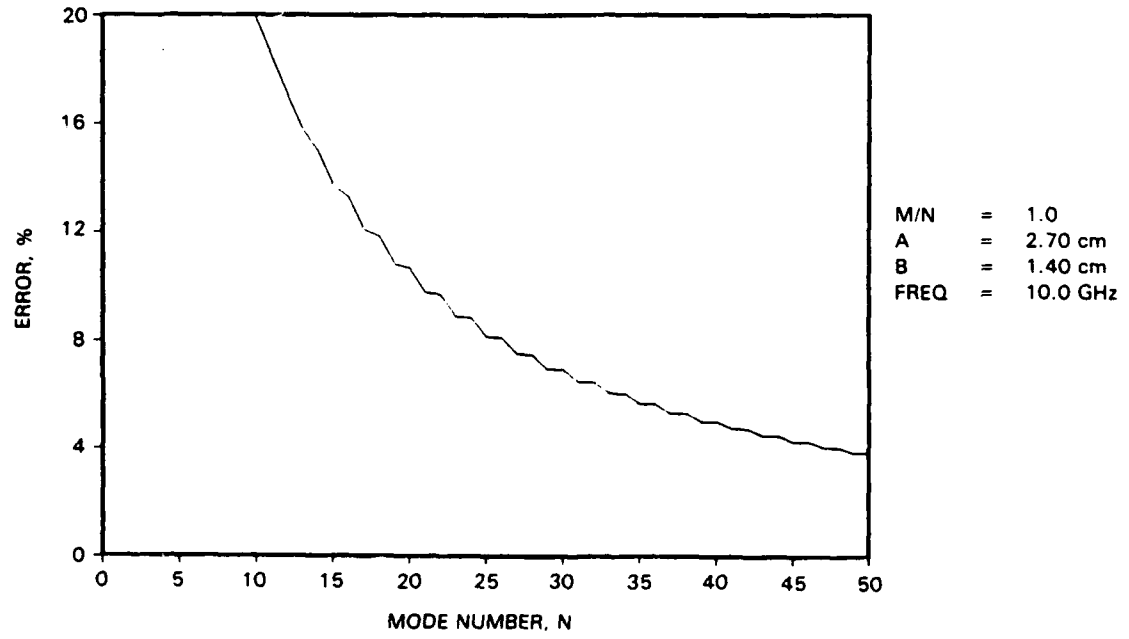


FIGURE 24. Error Versus Mode Number for Parallel-Plate Waveguide Junction (Modal Ratio of 1).

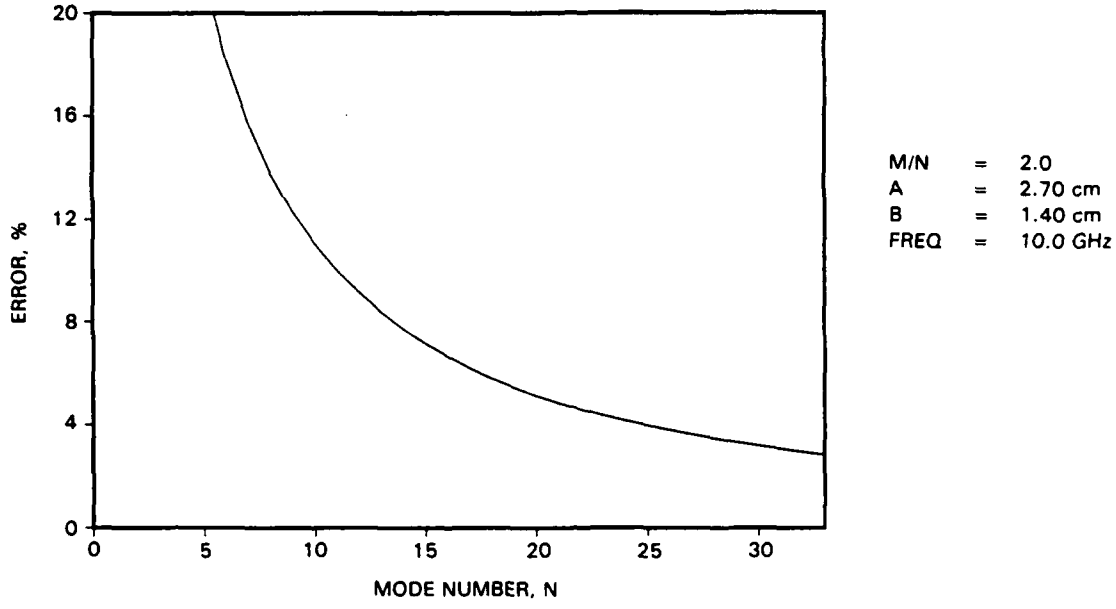


FIGURE 25. Error Versus Mode Number for Parallel-Plate Waveguide Junction (Modal Ratio of 2).

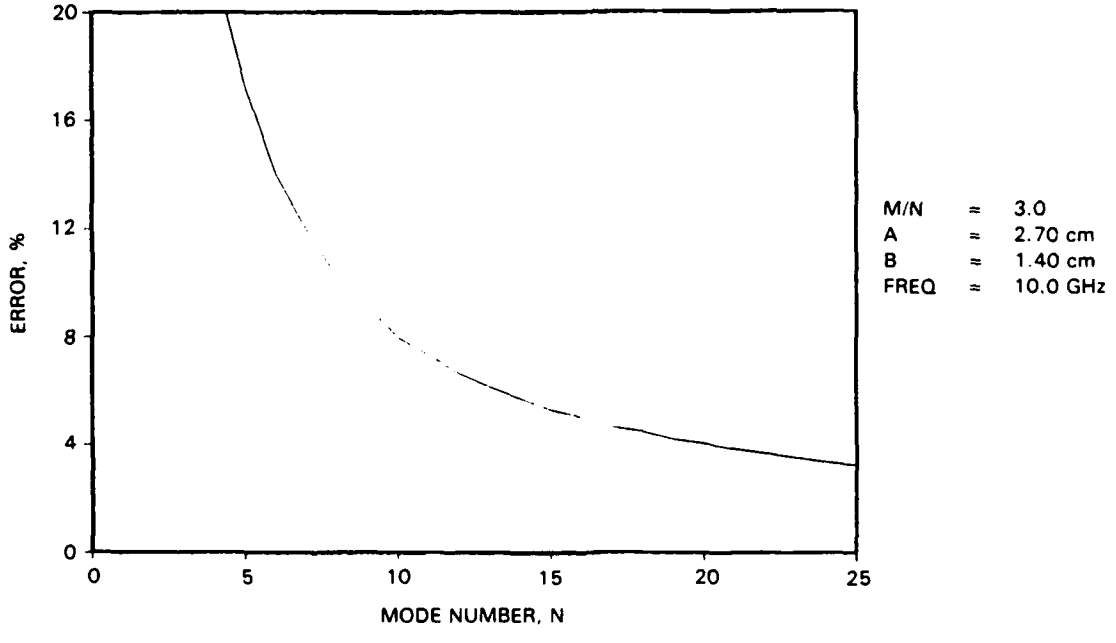


FIGURE 26. Error Versus Mode Number for Parallel-Plate Waveguide Junction (Modal Ratio of 3).

# Appendix A

## A CAPACITIVE IRIS IN A PARALLEL-PLATE WAVEGUIDE

Consider the simple capacitive iris discontinuity in a symmetric parallel-plate waveguide (References 13 and 20) (see Figure A-1).

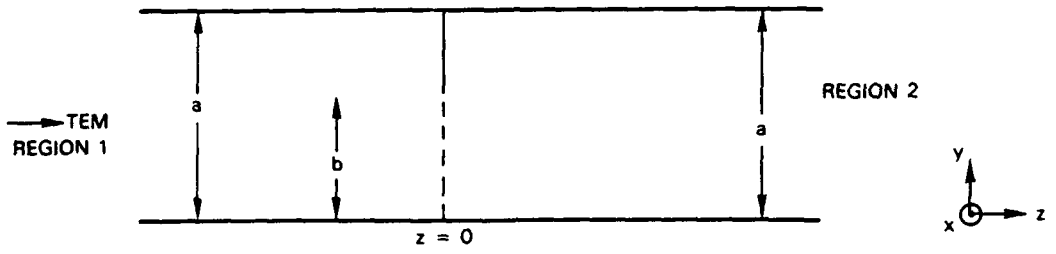


FIGURE A-1. Geometry for the Infinitely Thin Capacitive Iris in a Parallel-Plate Waveguide.

The following assumptions are made: (1) Only transverse electromagnetic (TEM) mode incidence exists (from the left); (2) both regions extend to infinity; (3) only higher order transverse magnetic (TM) modes are generated by the discontinuity; (4) all $\partial/\partial x = 0$, since the waveguide extends to infinity along the x coordinate; and (5) $\varepsilon = \varepsilon_o$ and $\mu = \mu_o$ inside the guide.

Assumption (1) indicates that

$$a_o^{(1)} \equiv 1$$

$$a_m^{(1)} = 0 \quad ; \quad m > 0 \qquad \text{(A-1)}$$

(The value of 1 is arbitrarily chosen.)

Assumption (2) implies that

$$a_p^{(2)} \equiv 0 \quad ; \quad \forall\, p \tag{A-2}$$

The only nonzero field components are $E_z$, $H_x$, and $E_y$ from assumptions (3) and (4). The normalized tangential fields in region 1 are well known to be (Reference 13)

$$E_y^{(1)} = \sqrt{\frac{\varepsilon_o^{(1)}}{a}}\, a_o^{(1)}\, e^{-\gamma_o^{(1)} z} + \sum_{m=0}^{\infty} b_m^{(1)} \sqrt{\frac{\varepsilon_m^{(1)}}{a}} \cos\frac{m\pi y}{a}\, e^{\gamma_m^{(1)} z} \tag{A-3a}$$

$$Z_o\, H_x^{(1)} = -\sqrt{\frac{\varepsilon_o^{(1)}}{a}}\, a_o^{(1)}\, e^{-\gamma_o^{(1)} z} + \sum_{m=0}^{\infty} b_m^{(1)} \sqrt{\frac{\varepsilon_m^{(1)}}{a}}\, Y_m^{(1)} \cos\frac{m\pi y}{a}\, e^{\gamma_m^{(1)} z} \quad ; \quad z < 0 \tag{A-3b}$$

while the fields in region 2 are

$$E_y^{(2)} = \sum_{p=0}^{\infty} b_p^{(2)} \sqrt{\frac{\varepsilon_p^{(2)}}{a}} \cos\frac{p\pi y}{a}\, e^{-\gamma_p^{(2)} z} \tag{A-4a}$$

$$Z_o H_x^{(2)} = -\sum_{p=0}^{\infty} b_p^{(2)} \sqrt{\frac{\varepsilon_p^{(2)}}{a}}\, Y_p^{(2)} \cos\frac{p\pi y}{a}\, e^{-\gamma_p^{(2)} z} \quad ; \quad z > 0 \tag{A-4b}$$

where

$$\varepsilon_j^{(k)} = \begin{cases} 1 \ ; \ j = 0 \\ \qquad ; \ \text{if } k = 1, j = m \text{ or if } k = 2, j = p \\ 2 \ ; \ j > 0 \end{cases} \tag{A-5}$$

and the normalized wave admittances in each region are

$$Y_j^{(k)} = \frac{i}{\sqrt{\left(\frac{j\lambda_o}{2a}\right)^2 - 1}} \ ; \ \text{if } k = 1, j = m \text{ or if } k = 2, j = p \tag{A-6}$$

($Z_o$ is the free-space impedance.) The boundary conditions at z = 0 are

$$E_y^{(1)} = 0 \ ; \ b < y < a \tag{A-7a}$$

$$E_y^{(2)} = 0 \ ; \ b < y < a \tag{A-7b}$$

$$E_y^{(1)} = E_y^{(2)} \ ; \ 0 < y < b \tag{A-7c}$$

$$H_x^{(1)} = H_x^{(2)} \ ; \ 0 < y < b \tag{A-7d}$$

Substituting Equations 3 and 4 into 7, the boundary conditions become

$$\sqrt{\frac{1}{a}}\, a_0^{(1)} + \sum_{m=0}^{\infty} b_m^{(1)} \sqrt{\frac{\varepsilon_m^{(1)}}{a}} \cos\frac{m\pi y}{a} - \sum_{p=0}^{\infty} b_p^{(2)} \sqrt{\frac{\varepsilon_p^{(2)}}{a}} \cos\frac{p\pi y}{a} = 0 \quad ; \quad 0 < y < b \tag{A-8a}$$

$$-\sqrt{\frac{1}{a}}\, a_0^{(1)} + \sum_{m=0}^{\infty} b_m^{(1)} \sqrt{\frac{\varepsilon_m^{(1)}}{a}}\, Y_m^{(1)} \cos\frac{m\pi y}{a} + \sum_{p=0}^{\infty} b_p^{(2)} \sqrt{\frac{\varepsilon_p^{(2)}}{a}}\, Y_p^{(2)} \cos\frac{p\pi y}{a} = 0 \quad ; \quad 0 < y < b \tag{A-8b}$$

$$\sqrt{\frac{1}{a}}\, a_0^{(1)} + \sum_{m=0}^{\infty} b_m^{(1)} \sqrt{\frac{\varepsilon_m^{(1)}}{a}} \cos\frac{m\pi y}{a} = 0 \quad ; \quad b < y < a \tag{A-8c}$$

$$\sum_{p=0}^{\infty} b_p^{(2)} \sqrt{\frac{\varepsilon_p^{(2)}}{a}} \cos\frac{p\pi y}{a} = 0 \quad ; \quad b < y < a \tag{A-8d}$$

Let

$$\sqrt{\frac{\varepsilon_m^{(1)}}{a}} = N_m^{(1)} \ , \ \sqrt{\frac{\varepsilon_p^{(2)}}{a}} = N_p^{(2)} \tag{A-9a}$$

$$C_m^{(1)} = \cos\frac{m\pi y}{a} \ , \ C_p^{(2)} = \cos\frac{p\pi y}{a} \tag{A-9b}$$

In matrix form, Equation 8 becomes

$$\begin{pmatrix} N_m^{(1)} C_m^{(1)} & -N_p^{(2)} C_p^{(2)} \\ N_m^{(1)} C_m^{(1)} Y_m^{(1)} & N_p^{(2)} C_p^{(2)} Y_p^{(2)} \\ N_m^{(1)} C_m^{(1)} & 0 \\ 0 & N_p^{(2)} C_p^{(2)} \end{pmatrix} \begin{pmatrix} b_m^{(1)} \\ b_p^{(2)} \end{pmatrix} = \sqrt{\frac{1}{a}}\, a_0^{(1)} \begin{pmatrix} -1 \\ 1 \\ -1 \\ 0 \end{pmatrix} \tag{A-10}$$

or

$$Lb = Ma$$

The adjoint matrix to L is

$$L^{\dagger} = \begin{pmatrix} N_{m'}^{(1)} C_{m'}^{(1)} & N_{m'}^{(1)} C_{m'}^{(1)} Y_{m'}^{(1)*} & N_{m'}^{(1)} C_{m'}^{(1)} & 0 \\ -N_{p'}^{(2)} C_{p'}^{(2)} & N_{p'}^{(2)} C_{p'}^{(2)} Y_{p'}^{(2)*} & 0 & N_{p'}^{(2)} C_{p'}^{(2)} \end{pmatrix} \tag{A-11}$$

(m', p' are dummy indices).

The product $L^{\dagger}L$ must be integrated over the appropriate portion of the cross-sectional boundary where each of the original boundary conditions holds. Let

$$H = \int_C L^{\dagger} L \, dc \tag{A-12}$$

where C is the entire boundary at z = 0. We can write H in partitioned form as

$$H = \left(\begin{array}{c:c} H^{(11)} & H^{(12)} \\ \hdashline H^{(21)} & H^{(22)} \end{array}\right) \tag{A-13}$$

$H^{(11)}$ is formed by multiplying the first row of $L^{\dagger}$ by the first column of L and integrating, noting that m = 0 to ∞ ; m' = 0 to ∞.

$$H^{(11)} = \int_0^b N_{m'}^{(1)} N_m^{(1)} C_{m'}^{(1)} C_m^{(1)} \, dy + \int_0^b N_{m'}^{(1)} N_m^{(1)} C_{m'}^{(1)} C_m^{(1)} Y_m^{(1)} Y_{m'}^{(1)*} \, dy$$

$$+ \int_b^a N_{m'}^{(1)} N_m^{(1)} C_{m'}^{(1)} C_m^{(1)} \, dy \qquad \text{(A-14)}$$

$$H^{(11)} = N_{m'}^{(1)} N_m^{(1)} \left[ \int_0^a C_{m'}^{(1)} C_m^{(1)} \, dy + Y_m^{(1)} Y_{m'}^{(1)*} \int_0^b C_m^{(1)} C_{m'}^{(1)} \, dy \right] \qquad \text{(A-15)}$$

(See the end of this Appendix for evaluation of integrals.) Thus,

$$H^{(11)} = K_m + Y_m^{(1)} Y_{m'}^{(1)*} J_{mm'} \qquad \text{(A-16a)}$$

Without detail,

$$H^{(12)} = J_{m'p} \left[ Y_{m'}^{(1)*} Y_p^{(2)} - 1 \right] \qquad \text{(A-16b)}$$

$$H^{(21)} = J_{p'm} \left[ Y_{p'}^{(2)*} Y_m^{(1)} - 1 \right] \qquad \text{(A-16c)}$$

$$H^{(22)} = K_p + Y_{p'}^{(2)*} Y_p^{(2)} J_{pp'} \qquad \text{(A-16d)}$$

Thus $H^{(11)}$, $H^{(12)}$, $H^{(21)}$, and $H^{(22)}$ are matrices such that if m, m' run from 0 to M and p, p' run from 0 to P, then $H^{(11)}$ has dimensions (M + 1) by (M + 1), $H^{(12)}$ is (M + 1) by (P + 1), $H^{(21)}$ is (P + 1) by (M + 1), and $H^{(22)}$ is (P + 1) by (P + 1).

Of course, when M = P,

$$H^{(11)} = H^{(22)} \qquad \text{(A-17a)}$$

and

$$H^{(12)} = H^{(21)} \tag{A-17b}$$

because of the particular symmetry of this problem. To integrate the forcing function, we take

$$f = \int_c L^{\dagger} M \, dc$$

which is a column vector (see end of this Appendix for integrals),

$$f = \begin{pmatrix} f^{(1)} \\ --- \\ f^{(2)} \end{pmatrix} \tag{A-18}$$

with

$$f^{(1)} = -\delta_{m'} + Y^{(1)*}_{m'} \rho_{m'} \tag{A-19a}$$

$$f^{(2)} = \rho_{p'} [1 + Y^{(2)*}_{p'}] \tag{A-19b}$$

Once H and f are known, we can take the inverse of H and find the scattering matrix. Since only a single input was assumed, we obtain only one row and one column of the complete scattering matrix:

$$S = H^{-1} f \tag{A-20}$$

From previously, if

$$H b = f a \tag{A-21}$$

the set of unknown coefficients, $b^{(1)}$ and $b^{(2)}$, can be found independently using the partitioned form of H (References 21 and 22). Thus,

$$\begin{pmatrix} H^{(11)} & H^{(12)} \\ \hline H^{(21)} & H^{(22)} \end{pmatrix} \begin{pmatrix} b^{(1)} \\ \hline b^{(2)} \end{pmatrix} = \begin{pmatrix} f^{(1)} \\ \hline f^{(2)} \end{pmatrix} a_0^{(1)} \tag{A-22}$$

(Let $a_0{}^{(1)} = 1.$) Then

$$H^{(11)}\, b^{(1)} + H^{(12)}\, b^{(2)} = f^{(1)} \tag{A-23a}$$

$$H^{(21)}\, b^{(1)} + H^{(22)}\, b^{(2)} = f^{(2)} \tag{A-23b}$$

and

$$b^{(1)} = [H^{(11)} - H^{(12)}\, H^{(22)^{-1}}\, H^{(21)}]^{-1}\, [f^{(1)} - H^{(12)}\, H^{(22)^{-1}}\, f^{(2)}] \tag{A-24a}$$

$$b^{(2)} = [H^{(22)} - H^{(21)}\, H^{(11)^{-1}}\, H^{(12)}]^{-1}\, [f^{(2)} - H^{(21)}\, H^{(11)^{-1}}\, f^{(1)}] \tag{A-24b}$$

The reflection and transmission coefficients are $b^{(1)}$ and $b^{(2)}$, respectively, for the TEM plus all higher order TM modes. For computing purposes, rather than use Equations 24, it is easier to use

$$b = H^{-1}\, f \tag{A-25}$$

and find $b^{(1)}$ and $b^{(2)}$ simultaneously. H is an (M + P + 2) by (M + P + 2) matrix, while f is an (M + P + 2) column vector as is b.

## ORTHONORMALIZED INTEGRALS USED IN THE CAPACITIVE IRIS PROBLEM

Let

$$J_{mm'} = \frac{\sqrt{\varepsilon_m^{(1)}\varepsilon_{m'}^{(1)}}}{a}\int_o^b \cos\frac{m'\pi y}{a}\cos\frac{m\pi y}{a}\,dy \tag{A-26}$$

$$J_{mm'} = \begin{cases} \dfrac{b}{a} & ;\ m=0,\ m'=0 \\ \dfrac{\sqrt{2}}{m\pi}\sin\dfrac{m\pi b}{a} & ;\ m'=0,\ m\neq 0 \\ \dfrac{\sqrt{2}}{m'\pi}\sin\dfrac{m'\pi b}{a} & ;\ m'\neq 0,\ m=0 \\ \dfrac{b}{a} & ;\ m=m'\ (m,\ m'>0) \\ \dfrac{1}{a}\left\{\dfrac{\sin\left(\dfrac{m'\pi}{a}-\dfrac{m\pi}{a}\right)b}{\left(\dfrac{m'\pi}{a}-\dfrac{m\pi}{a}\right)}+\dfrac{\sin\left(\dfrac{m'\pi}{a}+\dfrac{m\pi}{a}\right)b}{\dfrac{m'\pi}{a}+\dfrac{m\pi}{a}}\right\} & \\ m\neq m';\ m'\neq 0,\ m\neq 0 & \end{cases} \tag{A-27}$$

$$K_m = \frac{\sqrt{\varepsilon_m^{(1)}\varepsilon_{m'}^{(1)}}}{a}\int_0^a \cos\frac{m'\pi y}{a}\cos\frac{m\pi y}{a}\,dy = \begin{cases} 0 & m\neq m' \\ 1 & m=m', \\ & m,\ m'>0 \\ 1 & m=m'=0 \end{cases} \tag{A-28}$$

$$J_{m'p} = \frac{\sqrt{\varepsilon_{m'}^{(1)}\varepsilon_p^{(2)}}}{a}\int_0^b \cos\frac{m'\pi y}{a}\cos\frac{p\pi y}{a}\,dy \tag{A-29}$$

(Same as Equation A-27 for $J_{mm'}$ with m' = m, p = m'.)

$$J_{p'm} = \frac{\sqrt{\varepsilon_{p'}^{(2)}\varepsilon_{m}^{(1)}}}{a}\int_0^b \cos\frac{m\pi y}{a}\cos\frac{p'\pi y}{a}\,dy \tag{A-30}$$

(Same as $J_{mm'}$ with p' = m, m = m'.) $J_{pp'} = J_{mm'}$ with p = m, p' = m'.

$$\delta_{m'} = \sqrt{\frac{\varepsilon_{m'}^{(1)}}{a}}\int_0^a \cos\frac{m'\pi y}{a}\,dy = \begin{cases} 0 \;;\; m' > 0 \\ \\ 1 \;;\; m' = 0 \end{cases} \tag{A-31}$$

$$\rho_{m'} = \sqrt{\frac{\varepsilon_{m'}^{(1)}}{a}}\int_0^b \cos\frac{m\pi y}{a}\,dy \tag{A-32}$$

or

$$\rho_{m'} = \begin{cases} \dfrac{b}{a} & ;\; m' = 0 \\ \\ \dfrac{\sqrt{2}}{m'\pi}\sin\dfrac{m'\pi b}{a} & ;\; m' > 0 \end{cases} \tag{A-33}$$

($\rho_{p'}$ is the same with m' = p'.)

## Appendix B

## THE ASYMMETRICAL H-PLANE PARALLEL-PLATE WAVEGUIDE STEP

Assume that the asymmetrical H-plane parallel-plate waveguide step is as shown in Figure B-1. The following assumptions are made: (1) There is $TE_{0\,1}$

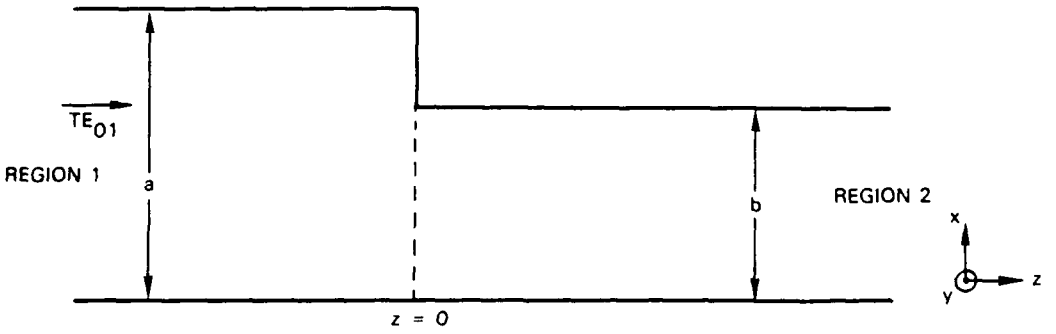


FIGURE B-1. Geometry for the Asymmetrical H-Plane Parallel-Plate Waveguide Step.

mode incidence from the left; (2) both regions extend to infinity; (3) only higher order TE modes are generated by the step; (4) all $\partial/\partial y = 0$; and (5) $\varepsilon = \varepsilon_o$, $\mu = \mu_o$ inside the guides.

We have (similar to Appendix A),

$$a_1^{(1)} \equiv 1$$

$$a_m^{(1)} = 0 \;;\; m > 1 \qquad \text{(B-1a)}$$

and

$$a_p^{(2)} \equiv 0 \;;\; \forall p \qquad \text{(B-1b)}$$

Nonzero components of the fields are $H_z$, $H_x$, and $E_y$. The normalized tangential fields in region 1 are

$$E_y^{(1)} = \sqrt{\frac{2}{a}} \sum_{m=1}^{\infty} [a_m^{(1)} e^{-\gamma_m^{(1)} z} + b_m^{(1)} e^{\gamma_m^{(1)} z}] \sin \frac{m\pi x}{a} \tag{B-2a}$$

$$Z_0 H_x^{(1)} = \sqrt{\frac{2}{a}} \sum_{m=1}^{\infty} Y_m^{(1)} [-a_m^{(1)} e^{-\gamma_m^{(1)} z} + b_m^{(1)} e^{\gamma_m^{(1)} z}] \sin \frac{m\pi x}{a} \quad ; \quad z < 0 \tag{B-2b}$$

and in region 2, they are

$$E_y^{(2)} = \sqrt{\frac{2}{b}} \sum_{p=1}^{\infty} b_p^{(2)} e^{-\gamma_p^{(2)} z} \sin \frac{p\pi x}{b} \quad ; \quad z > 0 \tag{B-3a}$$

$$Z_0 H_x^{(2)} = -\sqrt{\frac{2}{b}} \sum_{p=1}^{\infty} Y_p^{(2)} b_p^{(2)} e^{-\gamma_p^{(2)} z} \sin \frac{p\pi x}{b} \quad ; \quad z > 0 \tag{B-3b}$$

with the axial propagation constants given by

$$\gamma_m^{(1)} = \sqrt{\left(\frac{m\pi}{a}\right)^2 - k_o^2}$$

$$\gamma_p^{(2)} = \sqrt{\left(\frac{p\pi}{b}\right)^2 - k_o^2}$$

$$k_o = \omega\sqrt{\varepsilon_o \mu_o} \tag{B-4}$$

and the normalized admittances are

$$Y_m^{(1)} = \frac{i}{\sqrt{\left(\frac{m\lambda_o}{2a}\right)^2 - 1}} \quad ; \quad Y_p^{(2)} = \frac{i}{\sqrt{\left(\frac{p\lambda_o}{2b}\right)^2 - 1}} \tag{B-5}$$

The tangential boundary conditions used on z = 0 are

$$E_y^{(1)} = 0 \quad ; \quad b < x < a \tag{B-6a}$$

$$E_y^{(1)} = E_y^{(2)} \; ; \; 0 < x < b \tag{B-6b}$$

$$H_x^{(1)} = H_x^{(2)} \; ; \; 0 < x < b \tag{B-6c}$$

Substituting Equations B-2 and B-3 into B-6, we have

$$\sqrt{\frac{2}{a}}\left[a_1^{(1)} \sin\frac{\pi x}{a} + \sum_{m=1}^{\infty} b_m^{(1)} \sin\frac{m\pi x}{a}\right] = \sqrt{\frac{2}{b}} \sum_{p=1}^{\infty} b_p^{(2)} \sin\frac{p\pi x}{b} \; ; \; 0 < x < b \tag{B-7a}$$

$$\sqrt{\frac{2}{a}}\left[-a_1^{(1)} Y_1^{(1)} \sin\frac{\pi x}{a} + \sum_{m=1}^{\infty} Y_m^{(1)} b_m^{(1)} \sin\frac{m\pi x}{a}\right] = -\sqrt{\frac{2}{b}} \sum_{p=1}^{\infty} b_p^{(2)} Y_p^{(2)} \sin\frac{p\pi x}{b} \; ; \; 0 < x < b \tag{B-7b}$$

$$\sqrt{\frac{2}{a}}\left[a_1^{(1)}\sin\frac{\pi x}{a}+\sum_{m=1}^{\infty}b_m^{(1)}\sin\frac{m\pi x}{a}\right]=0 \qquad \text{(B-7c)}$$

In matrix form,

$$L=\begin{bmatrix}\sqrt{\frac{2}{a}}\sin\frac{m\pi x}{a} & -\sqrt{\frac{2}{b}}\sin\frac{p\pi x}{b}\\ \sqrt{\frac{2}{a}}\,Y_m^{(1)}\sin\frac{m\pi x}{a} & \sqrt{\frac{2}{b}}\,Y_p^{(2)}\sin\frac{p\pi x}{b}\\ \sqrt{\frac{2}{a}}\sin\frac{m\pi x}{a} & 0\end{bmatrix} \qquad \text{(B-8)}$$

and

$$L^{\dagger}=\begin{bmatrix}\sqrt{\frac{2}{a}}\sin\frac{m'\pi x}{a} & \sqrt{\frac{2}{a}}\,Y_{m'}^{(1)*}\sin\frac{m'\pi x}{a} & \sqrt{\frac{2}{a}}\sin\frac{m'\pi x}{a}\\ -\sqrt{\frac{2}{b}}\sin\frac{p'\pi x}{b} & \sqrt{\frac{2}{b}}\,Y_{p'}^{(2)*}\sin\frac{p'\pi x}{b} & 0\end{bmatrix} \qquad \text{(B-9)}$$

where m' and p' are dummy indices. Let the matrix

$$b=\begin{pmatrix}b^{(1)}\\ \hline b^{(2)}\end{pmatrix} \qquad \text{(B-10)}$$

contain the reflection and transmission coefficients for each mode and let the inputs be

$$Ma = a_1^{(1)} \begin{pmatrix} -\sqrt{\frac{2}{a}} \sin \frac{\pi x}{a} \\ \sqrt{\frac{2}{a}}\, Y_1^{(1)} \sin \frac{\pi x}{a} \\ -\sqrt{\frac{2}{a}} \sin \frac{\pi x}{a} \end{pmatrix} \quad ; \quad a_1^{(1)} = 1 \tag{B-11}$$

Let

$$H = \int_c L^{\dagger} L \, dc \tag{B-12}$$

As previously, we see that

$$H^{(11)} = \frac{2}{a} \int_o^a \sin \frac{m'\pi x}{a} \sin \frac{m\pi x}{a} \, dx + \frac{2}{a} Y_{m'}^{(1)*} Y_{m'}^{(1)} \times \int_o^b \sin \frac{m'\pi x}{a} \sin \frac{m\pi x}{a} \, dx \tag{B-13}$$

$$H^{(11)} = \begin{cases} 1 + Y_m^{(1)} Y_m^{(1)*} J_{mm} & ; \quad m = m' \\ Y_{m'}^{(1)*} Y_m^{(1)} J_{mm'} & ; \quad m \neq m' \end{cases} \tag{B-14a}$$

(For integrals, see end of this Appendix.) In similar fashion,

$$H^{(12)} = T_{m'p} \left[ Y_{m'}^{(1)*} Y_p^{(2)} - 1 \right] \tag{B-14b}$$

$$H^{(21)} = T_{mp'} \left[ Y_m^{(1)} Y_{p'}^{(2)*} - 1 \right] \tag{B-14c}$$

$$H^{(22)} = \begin{cases} 1 + Y_p^{(2)*} Y_p^{(2)} J_{pp} & ; \quad p = p' \\ Y_{p'}^{(2)*} Y_p^{(2)} J_{pp'} & ; \quad p \neq p' \end{cases} \tag{B-14d}$$

Again, let

$$f = \int_c L^\dagger M \, dc$$

where

$$f^{(1)} = \begin{cases} Y_1^{(1)} Y_{m'}^{(1)*} J_{1m'} & ; \quad m' \neq 1 \\ -1 + Y_1^{(1)} Y_1^{(1)*} J_{11} & ; \quad m' = 1 \end{cases} \tag{B-15a}$$

$$f^{(2)} = T_{1p'} [Y_1^{(1)} Y_{p'}^{(2)*} + 1] \tag{B-15b}$$

and

$$f = \begin{pmatrix} f^{(1)} \\ f^{(2)} \end{pmatrix} \tag{B-16}$$

Once H and f are found, we can compute the coefficients for the parallel-plate step just as in Appendix A.

## ORTHONORMALIZED INTEGRALS IN THE PARALLEL-PLATE STEP PROBLEM

Let

$$K_m = \frac{2}{a}\int_o^a \sin\frac{m'\pi x}{a}\sin\frac{m\pi x}{a}\,dx$$

$$= \begin{cases} 1 \quad ; \quad m = m' \\ 0 \quad ; \quad m \neq m' \end{cases} \tag{B-17}$$

$$J_{mm'} = \frac{2}{a}\int_o^b \sin\frac{m'\pi x}{a}\sin\frac{m\pi x}{a}\,dx$$

$$= \begin{cases} \dfrac{1}{a}\left[\dfrac{\sin(m'-m)\frac{\pi b}{a}}{(m'-m)\frac{\pi}{a}} - \dfrac{\sin(m'+m)\frac{\pi b}{a}}{(m'+m)\frac{\pi}{a}}\right] & ; \quad m \neq m' \\ \dfrac{b}{a} - \dfrac{\sin\frac{2m\pi b}{a}}{2m\pi} & ; \quad m = m' \end{cases} \tag{B-18}$$

$$T_{m'p} = \frac{2}{\sqrt{ab}} \int_o^b \sin \frac{m'\pi x}{a} \sin \frac{p\pi x}{b}\, dx$$

$$= \begin{cases} \dfrac{1}{\sqrt{ab}} \left[ \dfrac{\sin\left(\dfrac{m'\pi}{a} - \dfrac{p\pi}{b}\right) b}{\left(\dfrac{m'\pi}{a} - \dfrac{p\pi}{b}\right)} - \dfrac{\sin\left(\dfrac{m'\pi}{a} + \dfrac{p\pi}{b}\right) b}{\left(\dfrac{m'\pi}{a} + \dfrac{p\pi}{b}\right)} \right] ; \dfrac{m'}{a} \neq \dfrac{p}{b} \\ \left[ b - \dfrac{a \sin \dfrac{2m'\pi b}{a}}{2m'\pi} \right] ; \dfrac{m'}{a} = \dfrac{p}{b} \end{cases} \qquad \text{(B-19)}$$

($T_{mp'}$ and $J_{pp'}$ are same with proper correlation of indices.)

## Appendix C

## BOUNDARY CONDITIONS FOR THE PARALLEL-PLATE WAVEGUIDE

In general, if only a $TE_{01}$ mode is allowed to propagate in Figure C-1, there are only three nonzero field components, i.e., $E_y$, $H_x$, and $H_z$.

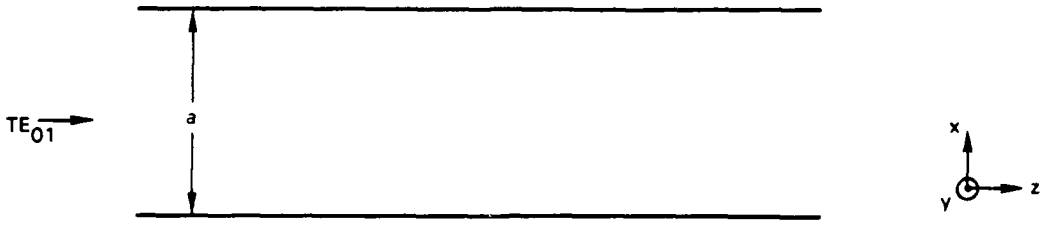


FIGURE C-1. Geometry for the Simple Parallel-Plate Waveguide With No Discontinuities.

If we assume that

$$E_y = A \sin \frac{\pi x}{a} e^{-\gamma z} \tag{C-1}$$

(since $E_y$ must be zero on both walls), then from Maxwell's curl equation,

$$\nabla \times \vec{E} = - i\omega\mu_o \vec{H} \tag{C-2}$$

$$H_x = \frac{1}{i\omega\mu_o} \frac{\partial E_y}{\partial z} \tag{C-3a}$$

and

$$H_z = -\frac{1}{i\omega\mu_o}\frac{\partial E_y}{\partial x} \tag{C-3b}$$

Similarly, from the other curl equation,

$$E_y = \frac{1}{i\omega\varepsilon_o}\left[\frac{\partial H_x}{\partial z} - \frac{\partial H_z}{\partial x}\right] \tag{C-4}$$

The divergence equations give

$$\frac{\partial E_y}{\partial y} \equiv 0 \tag{C-5a}$$

(simply the result of the two-dimensional nature of the problem) and

$$\frac{\partial H_x}{\partial x} + \frac{\partial H_z}{\partial z} = 0 \tag{C-5b}$$

Substituting Equation C-1 into C-3,

$$H_x = -\frac{\gamma}{i\omega\mu_o} E_y \tag{C-6a}$$

$$H_z = -\left(\frac{\pi}{a}\right)\frac{A}{i\omega\mu_o}\cos\frac{\pi x}{a}\, e^{-\gamma z} \tag{C-6b}$$

Now consider what happens when a discontinuity is introduced at z = 0; i.e., we use

(a) continuous tangential $\vec{E}$ and $\vec{H}$

(b) continuous normal $\vec{B}$ and $\vec{D}$

} for dielectric boundaries

and

(c) $\hat{n} \times \vec{E} = 0, \hat{n} \cdot \vec{B} = 0, \hat{n} \times \vec{H} = \vec{J}_s$ for perfectly conducting boundaries,

where $J_s$ is the surface current density. Thus, at the discontinuity (see Figure B-1),

$$
\begin{aligned}
&(1)\ E_y^{(1)} = E_y^{(2)} && \text{on } z = 0,\ 0 < x < b \\
&(2)\ E_y^{(1)} = 0 && \text{on } z = 0,\ b < x < a \\
&(3)\ H_x^{(1)} = H_x^{(2)} && \text{on } z = 0,\ 0 < x < b \\
&(4)\ H_z^{(1)} = H_z^{(2)} && \text{on } z = 0,\ 0 < x < b \\
&(5)\ H_z^{(1)} = 0 && \text{on } z = 0,\ b < x < a \\
&(6)\ H_x^{(1)} = J_s && \text{on } z = 0,\ b < x < a
\end{aligned}
\qquad \text{(C-7)}
$$

(We assume that $\vec{E}^{(2)}$, $\vec{H}^{(2)}$ do not exist for $x > b$.) Conditions (1), (2), (3), and (6) are tangential conditions; conditions (4) and (5) are normal conditions at the discontinuity. It is important to realize that in the least-squares boundary residual method (LSBRM), the tangential conditions are used to compute the scattering parameters and the statement is often made that the normal conditions are "equivalent" (Reference 14) to the tangential ones (the implication being that the normal conditions are satisfied automatically). While this may be true in some cases, in the present instance we see that there is not enough information from (4) and (5) alone to solve the problem. Attempts to mix appropriate tangential and normal conditions in the LSBRM formulation have not been successful.

In some treatments of the parallel-plate waveguide step, the boundary condition

$$
\frac{\partial H_x}{\partial z} = 0 \qquad \text{for } z = 0,\ b < x < a \qquad \text{(C-8)}
$$

is used along with the usual tangential conditions (References 23 and 24). This condition cannot be derived directly from (a), (b), or (c); however, indirectly, we recall from Equation C-4 that if $E_y = 0$ on some boundary, then

$$\frac{\partial H_x}{\partial z} - \frac{\partial H_z}{\partial x} = 0 \tag{C-9}$$

also, implying that both terms must either be equal to each other or both must be zero simultaneously. To use $\partial H_x/\partial z = 0$ without simultaneously using $\partial H_z/\partial x = 0$ is misleading.

## REFERENCES


1. N. Marcuvitz. *Waveguide Handbook.* New York, McGraw-Hill, 1951.

2. J. Schwinger and D. Saxon. *Discontinuities in Waveguides.* New York, Gordon and Breach Science Publishers, 1968.

3. L. Lewin. *Theory of Waveguides.* London, Butterworth, 1975.

4. R. Mittra. "Relative Convergence of a Doubly Infinite Set of Equations," *J. Res. Nat. Bur. Stand.*, Vol. 67D (1963), pp. 245-54.

5. A Wexler. "Solution of Waveguide Discontinuities by Modal Analysis," *IEEE Trans. Microwave Theory Tech.*, Vol. 15 (September 1967), pp. 508-17.

6. P. J. B. Clarricoats and K. R. Slinn. "Numerical Solution of Waveguide Discontinuity Problems," *Proc. IEE*, Vol. 114 (July 1967), pp. 878-86.

7. R. Mittra and S. W. Lee. *Analytical Techniques in the Theory of Guided Waves.* New York, Macmillian, 1971.

8. P. J. B. Clarricoats and A. B. Sharpe. "Modal Matching Applied to a Discontinuity in a Planar Surface Waveguide," *Electron. Lett.*, Vol. 8 (January 1972), pp. 28-29.

9. S. W. Lee, W. R. Jones, and J. J. Campbell. "Convergence of Numerical Solutions of Iris-Type Discontinuity Problems," *IEEE Trans. Microwave Theory Tech.*, Vol. 19 (June 1971), pp. 528-36.

10. J. Meixner. "The Behavior of Electromagnetic Fields at Edges," *IEEE Trans. Antennas Propag.*, Vol. 20 (July 1972), pp. 442-46.

11. C. Vassallo. "On a Direct Use of Edge Condition in Modal Analysis," *IEEE Trans. Microwave Theory Tech.*, Vol. 24 (April 1976), pp. 208-12.

12. M. Leroy. "On the Convergence of Numerical Results in Modal Analysis," *IEEE Trans. Antennas Propag.*, Vol. 31 (July 1983), pp. 655-59.

13. J. B. Davies. "A Least-Squares Boundary Residual Method for the Numerical Solution of Scattering Problems," *IEEE Trans. Microwave Theory Tech.*, Vol. 21 (February 1973), pp. 99-104.

14. H. Oraizi and J. Perini. "A Numerical Method for the Solution of the Junction of Cylindrical Waveguides," *IEEE Trans. Microwave Theory Tech.*, Vol. 21 (October 1973), pp. 640-42.

15. R. Jansen. "On the Performance of the Least Squares Method for Waveguide Junctions and Discontinuities," *IEEE Trans. Microwave Theory Tech.*, Vol. 23 (May 1975), pp. 434-36.

16. J. M. H. Olmsted. *Advanced Calculus.* New York, Appleton-Century-Crafts, 1956.

17. D. L. Powers. *Boundary Value Problems.* New York, Academic, 1972.

18. M. Becker. *The Principles and Applications of Variational Methods.* Cambridge, Massachusetts Institute of Technology Press, 1964.

19. B. A. Finlayson and L. E. Scriven. "The Method of Weighted Residuals - A Review," *App. Mech. Rev.*, Vol. 19 (September 1966), pp. 735-48.

20. R. E. Collin. *Field Theory of Guided Waves.* New York, McGraw-Hill, 1960.

21. S. A. Stigant. *The Elements of Determinants, Matrices, and Tensors for Engineers.* London, MacDonald, 1959.

22. W. J. Cole, E. R. Nagelburg, and C. M. Nagel. "Iterative Solution of Waveguide Discontinuity Problems," *Bell Syst. Tech. J.* (March 1967), pp. 649-72.

23. R. A. Waldron. *Theory of Guided Electromagnetic Waves.* London, Van Nostrand Reinhold, 1969.

24. W. L. Weeks. *Electromagnetic Theory for Engineering Applications.* New York, John Wiley and Sons, 1964.

INITIAL DISTRIBUTION

2 Naval Air Systems Command (AIR-5004)
2 Naval Sea Systems Command (SEA-09B312)
1 Commander in Chief, U. S. Pacific Fleet, Pearl Harbor (Code 325)
1 Commander, Third Fleet, San Francisco
1 Commander, Seventh Fleet, San Francisco
2 Naval Academy, Annapolis (Director of Research)
1 Naval War College, Newport
1 Air Force Intelligence Agency, Bolling Air Force Base (AFIA/INTAW, MAJ R. Esaw)
12 Defense Technical Information Center, Alexandria
1 Hudson Institute, Incorporated, Center for Naval Analyses, Alexandria, VA (Technical Library)
1 University of California, Riverside, CA (Prof. G. Everett)